# Chapter 7
# Taxonomic Discrimination of Phytoplankton by Spectral Fluorescence

Hugh L. MacIntyre, Evelyn Lawrenz, and Tammi L. Richardson

## 1 Introduction

Chlorophyll fluorescence techniques are used widely in both laboratory and field studies to assess the abundance and physiological responses of cyanobacteria, microalgae, macroalgae and vascular plants, as described in other chapters in this volume. Most of the instruments used in these studies excite fluorescence in the blue region of the spectrum and measure chlorophyll fluorescence (peak ca. 685 nm) at ambient temperature. Fluorescence is generally detected using a photomultiplier tube (PMT), which is very sensitive to intensity but insensitive to spectral quality. Cross-talk between the light source used to excite fluorescence and the detector is prevented by the use of cut-off filters on both the emitter and the PMT, or by the use of emitters with narrow wavebands, such as light-emitting diodes (LEDs) or lasers, and a long-pass filter on the detector. With the advent of LEDs, which have a very high efficiency (intensity of light output per unit power input) compared to the xenon flash-lamps used in many older instruments, commercially-available fluorometers can have very low power demands and be both small and sensitive (detection limits are typically <1 mg $m^{-3}$ of Chl*a*[1]). This makes them ideal for unattended monitoring such as on platforms, moorings or gliders.

Most such instruments use a single waveband to excite fluorescence and a single waveband to detect it. Those that use LEDs with peak emission at 460 or 470 nm excite Chl*a* fluorescence both directly and indirectly. Because the LED's emission spectrum has only a partial overlap with Chl*a*'s absorption spectrum (Fig. 1), direct excitation is less efficient than it would be for a light source with maximum emission at Chl*a*'s absorption peak at 440 nm. However, the 470 nm LED's emission is absorbed efficiently by the accessory *b* and *c* chlorophylls (Chl*b* and Chl*c*) and photosynthetic carotenoids (PSC) and is absorbed with much lower efficiency by phycoerythrins (PE). These can transfer the excitation energy to Chl*a*, which gives rise to its fluorescence. Although phycocyanins (PC) can also transfer energy to Chl*a*, their very low absorption of emission from the 470 nm LED (Fig. 1) would result in a negligible contribution to Chl*a*'s fluorescence with this excitation spectrum. Conversely, were the excitation delivered by

H.L. MacIntyre (✉)
Department of Oceanography, Dalhousie University, Halifax, NS B3H 4J1, Canada
e-mail: hugh.macintyre@dal.ca

E. Lawrenz and T.L. Richardson
Marine Science Program, University of South Carolina, Columbia, SC 29208, USA

T.L. Richardson
Department of Biological Sciences, University of South Carolina, Columbia, SC 29208, USA

[1] *Abbreviations*: AOA, Algae Online Analyzer (*bbe* Moldaenke); CCMP, Guillard-Provasoli Center for the Culture of Marine Phytoplankton (Boothbay Harbor, ME, USA); CFC, cellular fluorescence capacity, an analog of the maximum quantum yield of photosynthesis; Chl*a*, *b*, *c*; chlorophylls *a*, *b* and *c*; DPS, de-epoxidation state; FRR fast repetition rate (fluorometry); LHC, light-harvesting complex; $K_E$, saturating parameter of the growth-irradiance curve; MgDVP, Mg-3, 8-divinyl phaeoporphyrin $a_5$ monomethyl ester; NPQ, non-photochemical quenching; PAM, pulse amplitude modulated (fluorometry); PC, phycocyanin; PE, phycoerythrin; PPC, photoprotective carotenoids; PSC, photosynthetic carotenoids; PSI, photosystem I; PSII, photosystem II; SFS, spectral fluorescence signature(s)

D.J. Suggett et al. (eds.), *Chlorophyll* a *Fluorescence in Aquatic Sciences: Methods and Applications*, Developments in Applied Phycology 4, DOI 10.1007/978-90-481-9268-7_7, © Springer Science+Business Media B.V. 2010

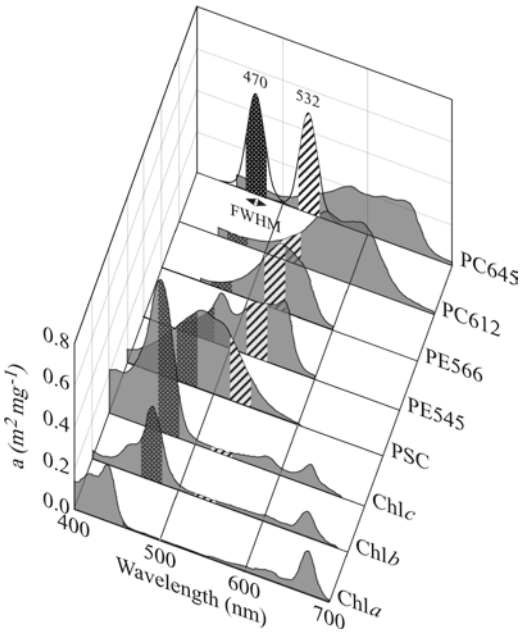


**Fig. 1** Absorption spectra for representative photosynthetic pigments. The emission spectra of two light sources, centered at 470 and 532 nm and each with 20 nm half-power bandwidth, are also shown. The bands corresponding to the full width at half maximum emission (FWHM) are superimposed on the absorption spectra. Spectra for chlorophylls and photosynthetic carotenoids (PSC) are approximations of absorption *in vivo* (Bidigare et al. 1990). Spectra for phycoerythrins (Hoef-Emden 2008) and phycocyanins (MacColl and Guard-Friar 1983) (PE and PC) are for absorption *in vitro*

an LED with maximum emission at 532 nm (Fig. 1), photosynthetic carotenoids and phycobilins would be able to absorb the excitation energy and transfer it to Chl*a*, resulting in Chl*a* fluorescence, but there would be negligible excitation of chlorophylls themselves.

Because the complement of accessory pigments varies between phytoplankton taxa, differences in the wavelengths at which Chl*a* fluorescence is stimulated and/or differences in the emission spectra have been used to infer taxonomic structure. Taxonomic differences in the absorption and fluorescence excitation spectra were described more than 50 years ago (Haxo and Blinks 1950; McLeod 1958) and have been documented in depth since (e.g. Neori et al. 1988; Johnsen and Sakshaug 2007). Spectral fluorescence as a discriminatory tool was first applied to phytoplankton in the late 1970s, notably by Yentsch and co-workers (Yentsch and Yentsch 1979; Yentsch and Phinney 1985), and the technique has since been developed extensively, largely by research groups in Estonia (Poryvkina et al. 1994; 2000; Babichenko et al. 1999; 2000); Germany (Kolbowski and Schreiber 1995; Gerhardt and Balode 1998; Beutler et al. 2002; 2003; 2004; Bodemer 2004; Jakob et al. 2005) and Finland (Seppälä and Balode 1998; Seppälä et al. 2007; Seppälä and Olli 2008). The technique has also been proposed to assay community structure in macroalgae (Topinka et al. 1990; Kieleck et al. 2001) and benthic microalgae (Gerhardt and Balode 1998; Aberle et al. 2006). Integrated multi-channel fluorometers are available commercially from several manufacturers, including Walz (Effeltrich, Germany), *bbe* Moldaenke (Kiel, Germany), Photon Systems Instruments (Brno, Czech Republic), LDI[3] (Tallinn, Estonia) and JFE ALEC (Kobe, Japan). Most approaches use excitation of Chl*a* fluorescence at multiple wavelengths but others have used excitation-emission matrices (Oldham et al. 1985; Desiderio et al. 1997; Zhang et al. 2006). In what follows, we review the principles of taxonomic fingerprinting by spectral fluorescence in microalgae and cyanobacteria. We do not address the application of spectral fluorescence in other contexts, such as flow cytometry (see Sosik et al., Chapter 8, this volume) or differentiation of corals (Mazel 1995), nor do we consider the applications of specialized techniques, such as picosecond time-resolved fluorescence spectra, 88 K fluorescence spectra or fluorescence recovery after bleaching, that are used to investigate energy transfer between pigments, state transitions and protein mobility (reviewed by Allen and Mullineaux 2004; Mimuro 2005).

## 2 The Principles of Taxonomy by Spectral Fluorescence

The intensity of fluorescence excited by a given light source can be expressed in general terms as:

$$Fl^{Chl}(\lambda_{Em}) = \sum \left[ E(\lambda_{Ex}) \bullet a_{PS}^{Chl}(\lambda_{Ex}) \right] \phi(\lambda_{Ex,Em}) \quad (1)$$

where $Fl^{Chl}(\lambda_{Em})$ is the Chl*a*-specific fluorescence intensity at emission wavelength $\lambda_{Em}$; $E(\lambda_{Ex})$ is the intensity of the excitation at wavelength $\lambda_{Ex}$; $a_{PS}^{Chl}(\lambda_{Ex})$ is the Chl*a*-specific absorption coefficient by photosynthetic pigments at $\lambda_{Ex}$; and $\phi(\lambda_{Ex,Em})$ is the effective quantum yield of fluorescence for the given excitation and emission wavelengths. Of these terms, differences in the excitation source and the optical geometry of the detector largely determine $E(\lambda_{Ex})$. Secondary variations arise from the presence of other optically-active

materials (i.e., those that absorb and scatter light) within the interrogation volume. The effective Chl*a*-specific absorption coefficient integrates both direct absorption by Chl*a* and absorption by accessory pigments that transfer energy to it. Its magnitude varies with wavelength, as specified, and with both genotypic and phenotypic variability in pigment complement and the degree of pigment packaging. Last, the effective quantum yield of fluorescence at the given excitation/emission wavelengths also depends on the proportion of energy that is directed to photosynthesis vs fluorescence vs other energy-dissipating pathways, which is under both genotypic and phenotypic control. It also depends on the degree to which the fluorescence emission is re-absorbed by the pigments and absorbed or scattered by any other optically-active materials in the interrogation volume. We consider below how variability in these parameters determines the degree to which spectral fluorescence measurements can be used to estimate the abundance and taxonomic affiliations of a phytoplankton assemblage.

## 2.1 Energy Transfer Between Pigments

As described in Eq. 1, fluorescence emission depends in part on the wavelength-dependence of the photosynthetic absorption coefficient, $a_{PS}^{Chl}$. Because room-temperature fluorescence at 680–690 nm, which is the standard window for commercial instruments, is dominated by fluorescence from PSII, (see Itoh and Sugiura 2004), it is more accurate to say that it depends on the photosynthetic absorption cross-section of PSII. This in turn is related to the effective photosynthetic cross-section per reaction center (σ in darkness and σ′ in the presence of actinic illumination) via the size of the pigment antenna, which is the mean number of pigment molecules associated with each reaction center. Both σ and σ′ can be estimated by curve-fitting the dependence of fluorescence intensity on excitation intensity at a given waveband, using an FRR fluorometer (Laney 2003; Laney and Letelier 2008); σ can also be estimated by spectral correction of the absorption cross-section for the contribution of non-photosynthetic pigments, given a specified distribution of pigments between PSI and PSII (Suggett et al. 2004).

The mechanisms of energy transfer between pigments have been reviewed in detail by Falkowski and Raven (2007), and what follows reiterates their account. Absorption of light energy by Chl*a* raises an electron

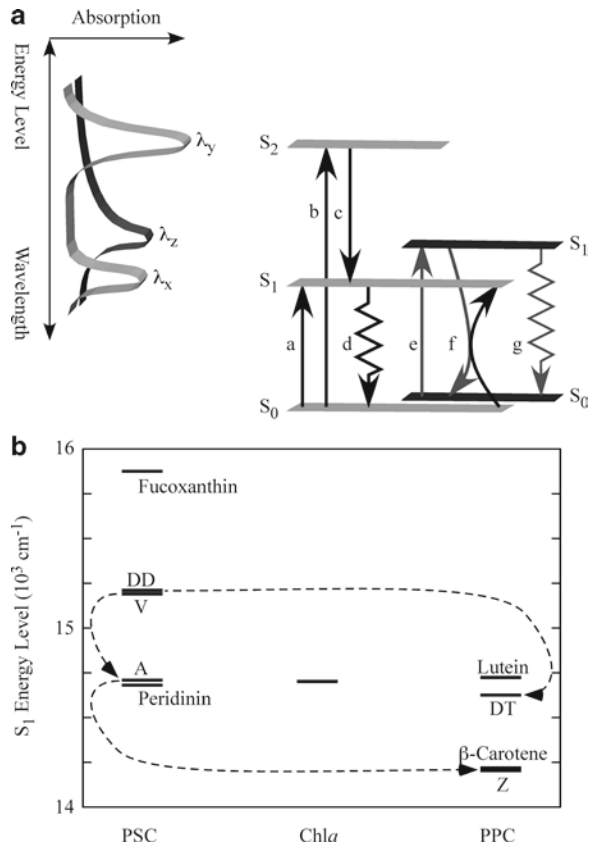


**Fig. 2** (**a**) Schematic representation of electron energy levels and corresponding absorption bands for Chl*a* and an accessory pigment, shown as light and dark grey, respectively (modified from Falkowski and Raven 2007). *a, b, e*: raise in electron energy to the $S_1$ or $S_2$ level after absorption of a photon. *c*: spontaneous decay from the $S_2$ to $S_1$ level. *d, g*: decay from the $S_1$ to $S_0$ level, with emission of fluorescence. *f*: exciton migration. (**b**) Modeled $S_1$ energy levels of select photosynthetic and photoprotective carotenoids (PSC and PPC), relative to Chl*a*. Data are from Frank et al. (1997). Dotted arrows show the inter-conversion by de-epoxidation of the xanthophylls violaxanthin, antheraxanthin and zeaxanthin (V, A and Z) and diadinoxanthin and diatoxanthin (DD and DT)

from its ground state, $S_0$, to either the $S_1$ or $S_2$ level, indicated by *a* and *b* in Fig. 2a. Note that the absorption maxima for each pigment in Fig. 1 correspond to the energy required to achieve these changes, as a photon's energy declines with wavelength. An electron at the $S_2$ level drops rapidly to the $S_1$ level (*c* in Fig. 2a). From the $S_1$ level, the electron may either return to the ground state (*d* in Fig. 2a), emitting radiation with a lower energy and longer wavelength (i.e., fluorescence) or by transferring its energy to another Chl*a* molecule in raising its electron to the $S_1$ level. The latter is termed "exciton migration" and refers to the transfer of the energy associated with the electron, not migration of the

electron itself (i.e., ionization). Exciton migration can also occur between accessory pigments and Chl*a*. In the example that is shown, a pigment with an $S_1$ energy level higher than Chl*a*'s (e.g., PC) can absorb energy at wavelengths intermediate between the blue and red peaks of Chl*a*'s absorption spectrum (*e* in Fig. 2). If the $S_1$ energy band overlaps Chl*a*'s, exciton migration can occur between the accessory pigment and Chl*a* (*f* in Fig. 2), extending Chl*a*'s effective absorption spectrum and so contributing to the photosynthetic absorption cross-section ($a_{PS}^{Chl}$ in Eq. 1). In the absence of exciton migration, the accessory pigment's excited electron may also return to the ground state with a loss of energy as fluorescence (*g* in Fig. 2a).

The phycobilins have easily-observed fluorescence peaks. Because these reflect $S_1$ levels with higher energies than Chl*a*'s, the fluorescence has a correspondingly shorter wavelength. Although carotenoids do fluoresce, their quantum yields of fluorescence are very low and can not be detected with most instruments (Mimuro 2005). Their dominant absorption peak, centered at about 500 nm (Fig. 1), corresponds to the $S_2$ energy level. The $S_1$ energy levels are optically forbidden and so lack corresponding absorption peaks. The energy level of the $S_1$ state determines whether the carotenoid is photosynthetic or photoprotective. Because entropy does not permit exciton migration from a lower to a higher $S_1$ level, the energy transfer is unidirectional. Carotenoids with an $S_1$ level that is higher than but still overlapping with Chl*a*'s can transfer energy to it and, like the phycobilins, contribute directly to the spectral dependence of the photosynthetic absorption cross-section ($a_{PS}^{Chl}$). In contrast, those with an $S_1$ level that is lower than, but still overlapping with, Chl*a*'s can only accept electrons from it. These carotenoids absorb light but do not contribute to the photosynthetic cross-section and account for much of the difference between absorption and PSII fluorescence excitation spectra (see Lutz et al. 2001; Suggett et al. 2004). The cooperativity between photosynthetic carotenoids and Chl*a* has been visualized by comparing the excitation spectra of isolated Chl*a*-Chl*c*-peridinin binding proteins, functioning thylakoid micelles and whole cells (Jovine et al. 1995; Johnsen et al. 1997).

The modeled $S_1$ energy levels for several common carotenoids (Frank et al. 1997) are shown in Fig. 2b. Note that the $S_1$ energy level modeled for peridinin is lower than Chl*a*'s while lutein's is higher, although peridinin does transfer excitons to Chl*a* and lutein does not. The classification into photosynthetic and photoprotective groups is based on more direct means of estimating energy flow between Chl*a* and carotenoids such as picosecond time-resolved fluorescence spectroscopy (Mimuro 2005) and resonance Raman spectroscopy (Ruban et al. 2007), rather than the modeled energy levels alone.

## 2.2 Taxonomic Differences in Fluorescence Spectra

Taxonomic differences in the complement of PSII accessory pigments determine the differences in both the fluorescence excitation and emission spectra that are illustrated in Fig. 3. The fluorescence excitation spectra of a representative chlorophyte (*Dunaliella tertiolecta*), chromophyte (the diatoms *Chaetoceros muelleri* and *C. affinis*) and cryptophyte (*Storeatula major*) differ most obviously in the region between 500 and 600 nm. This is a consequence of differences in the complement of photosynthetic accessory pigments: the non-photosynthetic (photoprotective) carotenoids are distributed across taxa but do not contribute to the excitation spectra (Johnsen and Sakshaug 2007). In the chlorophyte, the carotenoids are dominated by lutein and β-carotene, both of which are photoprotective (see Fig. 2b) and therefore do not contribute to the excitation spectrum. Dominance of the carotenoid pool by photoprotective forms is also found across the chlorophyte lineages (the Prasinophyceae, Chlorophyceae, Euglenophyceae and Eustigmatophyceae, Jeffrey et al. 1997). The exception is for those taxa that contain siphonaxanthin, which is a major carotenoid in some Siphonales (e.g. Benson and Cobb 1981) and which may occur in some Micromonadophyceae (Fawley and Lee 1990; Wright et al. 1991). Variation in the shape of the excitation spectra within the chlorophytes is driven primarily by the relative amounts of Chl*a* and the accessory chlorophylls, Chl*b* and, in some prasinophytes, MgDVP (Jeffrey et al. 1997). The latter is an analog of Chl*c* and can give rise to pronounced secondary peaks in the excitation and emission spectra at c. 470 and 650 nm, respectively (Haxo and Blinks 1950), particularly when present in high quantities (e.g. in some prasinophytes, see Suggett et al. 2004; Johnsen and Sakshaug 2007).

The diatoms in Fig. 3 have relatively high quotas of the photosynthetic carotenoid fucoxanthin, which

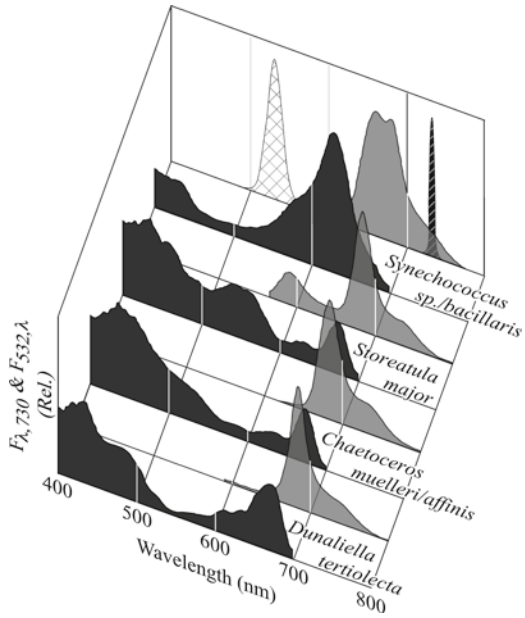


**Fig. 3** Fluorescence excitation and emission spectra (dark and light grey, respectively) for a representative chlorophyte (*Dunaliella tertiolecta*), chromophytes (the diatoms *Chaetoceros muelleri*, excitation, and *C. affinis*, emission), cryptophyte (*Storeatula major*) and phycocyanin-rich cyanobacteria (*Synechococcus sp*., excitation, and *S. bacillaris*, emission). Excitation spectra (dark grey) were driven with a variable excitation and detected at 730 nm (hatched spectrum on the back panel). Emission spectra (light grey) were driven with a 532 nm laser (cross-hatched spectrum on the back panel) and detected with a charge-coupled device. Excitation spectra are from Suggett et al. (2004). Emission spectra are unpublished data (MacIntyre and R. Cox)

contributes to $a_{PS}^{Chl}$ and accounts for the higher fluorescence excitation at 500–530 nm relative to that of the chlorophyte. Fucoxanthin and its derivatives, 19′-hexanoyloxyfucoxanthin and 19′-butanoyloxyfucoxanthin, or peridinin are found in all the chromophytic lineages (the Coscinodiscophyceae, Bacillariophyceae, Prymnesiophyceae, Chrysophyceae, Raphidophyceae, Pelagophyceae, Dinophyceae and Phaeophyceae. Hooks et al. 1988; Andersen et al. 1996; Jeffrey and Vesk 1997). In both the chlorophyte and diatom, the fluorescence emission spectrum is similar, with a single dominant peak at c. 680 nm attributable to Chl*a*. The peak wavelength can vary by 10 nm or more (Millie et al. 2002; Johnsen and Sakshaug 2007), which has been ascribed to differences in pigment-protein binding between taxa.

The excitation and emission spectra for the cryptophyte differ from those of the chlorophyte and chromophyte in having a marked peak in the excitation at c 550 nm and a second distinct peak in the emission spectrum at c. 590 nm (Fig. 3). These are due to the presence of phycobilins, in this case a PE (see Fig. 1), which give members of the class their characteristic colors. In most cryptophyte lineages, which are pink to brown in appearance, the phycobilins are PEs but some contain PCs (Hoef-Emden 2008) and may be blue-green.

Although the rhodophytes (not shown) and cyanobacteria also have Chl*a* and phycobilins as the photosynthetic pigments, they are unlike cryptophytes in lacking *c* chlorophylls. The Prochlorococcales are an exception among the cyanobacteria with regard to accessory chlorophylls, as they also contain divinyl Chl*b* and divinyl Chl*a* (Burger-Wiersma and Post 1989; Chisholm et al. 1992). The differences in excitation spectra between the cyanobacteria and cryptophytes arise both from differences in the pigments (Apt et al. 1995) and their arrangement in phycobilisomes in the cyanobacteria (and rhodophytes, which are not shown) vs. the LHC in the cryptophytes. The cyanobacterial PSII reaction center contains relatively small quantities of Chl*a* and light harvesting by PSII is dominated by the bilins in the phycobilisome. Chlorophyll *a* is primarily associated with PSI in cyanobacteria, it makes little contribution to the PSII excitation spectrum (Lutz et al. 2001; Suggett et al. 2004; Johnsen and Sakshaug 2007). In contrast to cyanobacteria, the phycobilins in cryptophytes are packed inside the thylakoid lumen (Spear-Bernstein and Miller 1989) and transfer energy efficiently to both PSI and PSII (Wit et al. 2008). There can also be significant differences between the emission spectra for cryptophytes and cyanobacteria. The spectra shown for the representative species in Fig. 3 are for a PE-containing cryptophyte and a PC-rich cyanobacterium. The latter lacks the 590 nm emission peak of PE and has instead a dominant peak at c. 655 nm due to PC. While both cryptophytes and cyanobacteria have PE-rich (pink) and PC-rich (blue-green) members, there are persistent differences in the excitation spectra because of the differences in the distribution of pigments in the phycobilisome vs the antenna/lumen and because of the presence of *c* chlorophylls as accessory pigments in the cryptophytes. There are also differences in the emission spectra of PE-rich representatives of the two classes because of taxonomic differences in the type of phycoerythrins (Apt et al. 1995). The PE emission

peak for the pink cyanobacteria *Synechococcus sp*. CCMP833 and *Synechocystis sp*. CCMP843 (not shown) was centered at c. 570 nm vs 590 nm in the cryptophytes *Storeatula major* (Fig. 3) and *Rhodomonas lens* CCMP739 (not shown).

Differences in both the excitation and emission spectra have been used to characterize the taxonomic structure of both microalgae and macroalgae *in vivo*. In many, if not most, cases, the approach has also been used to estimate the abundance of each group. We review the approach below, illustrating some potential pitfalls with experimental data.

## 2.3 Taxonomic Discrimination by Spectral Fluorescence

The basis of fluorometric taxonomic discrimination lies in classifying differences in fluorescence signatures that arise from consistent differences in pigment complement. Multiple approaches have been used that vary with the capabilities of the instruments at hand, but all rely on comparing the responses of unknown samples to the responses of representative taxa. At the simplest level, this can be achieved by examining the difference in emission, using excitation at two different wavelengths. This is illustrated in Fig. 4a, which shows discrimination between a diatom and a chlorophyte using the ratio of fluorescence excited at 530 and 450 nm (Yentsch and Yentsch 1979). The two wavelengths preferentially stimulate photosynthetic carotenoids (which the chlorophytes largely lack but which the diatoms have) and Chl*a* (Fig 1) and so the ratio exploits the dip in the chlorophyte's excitation spectrum relative to a diatom's at 530 nm (Fig. 3). The ratio approach works well in 2-species mixtures, but it has limited ability to discriminate between more complex mixtures, is sensitive to changes in background fluorescence, and is easily biased by acclimative changes in the representative organisms' excitation spectra (Oldham et al. 1985; Beeler SooHoo et al. 1986; Hilton et al. 1989).

By careful targeting of the regions of the spectra that have the highest between-taxon variability (Hilton et al. 1988), a fairly high degree of discrimination can be achieved with as few as 3–5 excitation wavelengths and a single emission wavelength. This is illustrated in Fig. 4b, which shows a cluster analysis of the spectral signatures of 44 strains of microalgae from seven classes, which were generated by excitation at 410, 510 and 540 nm (Gaevsky et al. 2005). The spectral fluorescence signatures (SFS) were reported as the ratios of $Fl_{540}$:$Fl_{410}$, $Fl_{510}$:$Fl_{410}$ and $Fl_{510}$:$Fl_{540}$, which were standardized to the mean value before constructing a matrix of pair-wise Bray-Curtis similarity coefficients in PRIMER-E (Clarke and Warwicke 2001). With three exceptions, the cultures clustered into three taxonomically-appropriate groups; chromophytes (almost all the diatoms and the dinoflagellates), chlorophytes (the chlorophytes *sensu stricto*, euglenophytes and xanthophytes) and the cyanobacteria. The lone cryptophyte and two of the diatoms clustered with the cyanobacteria. The dispersion within and between these groups is shown in a multidimensional scaling (MDS) plot (Fig. 4c) that is based, like the cluster analysis, on the matrix of pair-wise similarity coefficients. The ordination is analogous to a 2-D plot of principal components based on fully spectral or discrete data (Zhang et al. 2006; Seppälä and Olli 2008); the differences being that MDS plots can be based on non-parametric variables, are not scaled and are explicitly multivariate (in this case a 2-D representation of a 43-dimensional distribution rather than of just the first two dimensions of a multi-dimensional distribution). The spatial distribution is a representation of difference, in which distance between samples is inversely proportional to their similarity. Note that while the cryptophyte clusters with the cyanobacteria at 80% similarity, it forms an out-group with one of the two anomalous diatoms, *Synedra sp*., found within the cyanobacterial cluster (Fig. 4c).

The discriminatory power of the approach can be assessed by subjecting subsets of the similarity matrix to the permutative ANOSIM analysis, which is analogous to *a posteriori* pair-wise testing of differences after univariate 1-way Analysis of Variance, to test for significant differences. (The subsets are defined *a priori* as the taxonomic groups, rather than the groupings from the cluster analysis, to avoid a circular argument.) There are highly significant ($p < 0.001$) differences between the three groups that contain enough samples to give unbiased results, the chlorophytes, diatoms, and cyanobacteria (Table 1). The small sample sizes of the remaining groups precludes high confidence but their similarities to their taxonomic affiliates (dinoflagellates to diatoms, euglenophytes and xanthophytes to chlorophytes) are

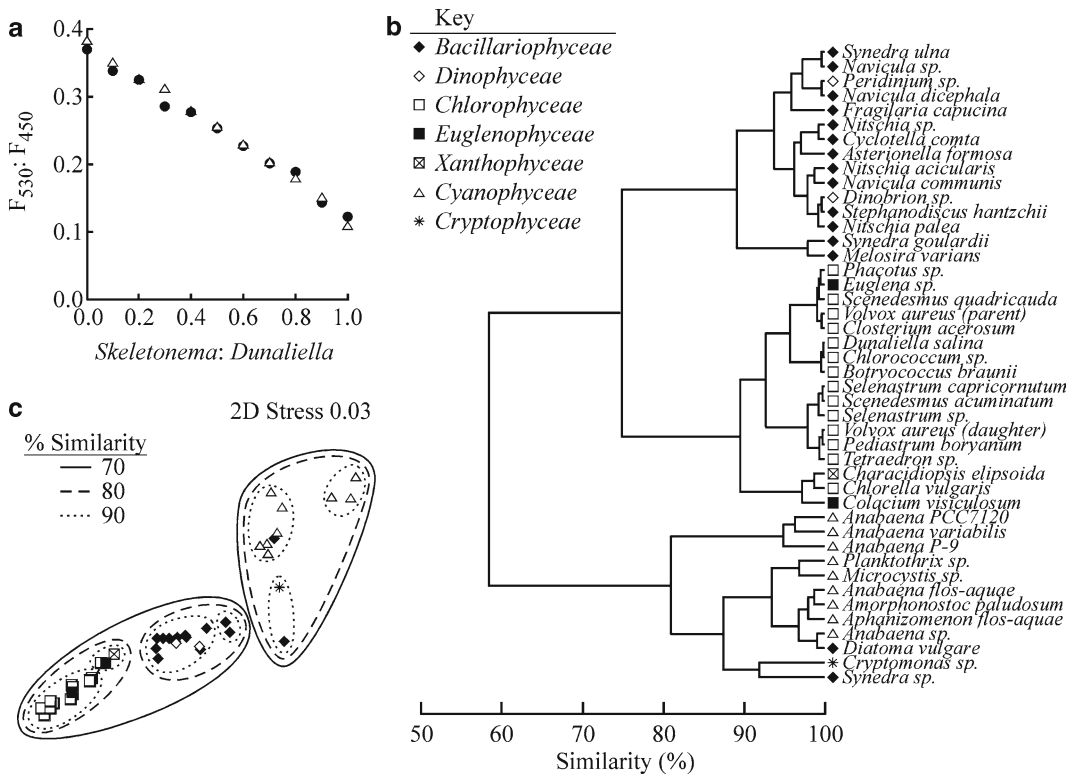


**Fig. 4** (**a**) Changes in the ratio of $Fl_{530}$:$F_{450}$ in binary mixtures of the diatom *Skeletonema costatum* and the chlorophyte *Dunaliella tertiolecta* (redrawn from Yentsch and Yentsch 1979). Circles and triangles represent replicated experiments. (**b**) Cluster analysis of average species- or strain-specific fluorescence signatures of 44 cyanobacteria and microalgae. Each signature is the average of 3 – 107 replicates. Data are from Gaevsky et al. (2005). See text for details of the analysis. (**c**) Dimensionless ordination of the similarity matrix from (b) in a multidimensional scaling plot (MDS). The distance between any pair of points is inversely proportional to their similarity. Contours are the similarity levels derived from the cluster analysis. The very low value of stress refers to the (minor) distortion imposed by reducing a 43-dimensional matrix to a 2-dimensional representation

comparable to the within-group similarities and their differences from taxonomic outgroups (dinoflagellates vs chlorophytes and cyanobacteria etc.) are also comparable to the differences between their affiliates and the out-groups (Table 1). Three conclusions can be drawn from the analysis of this data-set:

1. The spectral signatures reflect statistically-significant ($p < 0.01$) differences between organisms (Table 1)
2. There is variability within the statistically-different groups such that within-group similarity is less than 100% (i.e., signatures are not identical, Table 1) and
3. Outliers within the taxonomic groups can be classified as belonging to the wrong taxonomic group (Fig 4b, c)

The within-group variability means that classification between groups would probably best be handled by fuzzy logic, although to our knowledge, the approach has yet to be used. Instead, a variety of statistical techniques has been employed to analyze the spectral signatures of an unknown sample in terms of the contributions of known taxa. The spectral signature may be based on a continuous excitation spectrum (Babichenko et al. 1994; Gerhardt and Balode 1998; Seppälä and Olli 2008), a continuous emission spectrum (Cowles et al. 1993), and either a full (Oldham et al. 1985) or reduced excitation/emission matrix (Desiderio et al. 1997; Zhang et al. 2006). Because of the high level of redundancy in the spectra and matrices, comparable discriminatory power can be derived from discrete measurements that target areas of maximum variability in the excitation spectra (Kolbowski and Schreiber 1995; Beutler et al. 2002, 2004; Parésys et al. 2005) or in both the excitation and emission spectra (Murphy and Cowles 1997). In the case of spectral data, the signal derived from an unknown sample can be analyzed to estimate the contributions of known

**Table 1** Similarity analysis of taxonomic clusters based on standardized SFS (Gaevsky et al. 2005). Groupings are based on taxonomy, not on the cluster analysis in Fig. 4 (i.e. *Diatoma vulgare* and *Synedra sp.* are grouped with the diatoms rather than the cyanobacteria). N refers to the number of taxa within the group, not to the number of samples analyzed within a species, which ranged from 3 to 107 (mean 27). Similarity is the within-group similarity, defined by the SIMPER test of PRIMER-E. Dissimilarity is between-group dissimilarity (= 100% – Similarity). Testing for between-group differences vs the groups with the highest replication (i.e., the Bacillariophyceae, Chlorophyceae and Cyanophyceae) was by ANOSIM. The ANOSIM R statistic and p level are reported for each pair-wise comparison. The ANOSIM test was only run for those groups in which 55 or more permutative tests were possible (i.e., not for the Xanthophyceae and Cryptophyceae, which had only one representative each)

| | N | % Similarity | % Dissimilarity with Bacillariophyceae | % Dissimilarity with Chlorophyceae | % Dissimilarity with Cyanophyceae |
|---|---|---|---|---|---|
| Bacillariophyceae | 15 | 89.3 | | 29.4<br>R = 0.91; p < 0.001 | 28.6<br>R = 0.79; p < 0.001 |
| Chlorophyceae | 14 | 94.4 | 29.4<br>R = 0.91; p < 0.001 | | 56.0<br>R = 1.00; p < 0.001 |
| Cyanophyceae | 9 | 88.8 | 28.6<br>R = 0.79; p < 0.001 | 56.0<br>R = 1.00; p < 0.001 | |
| Dinophyceae | 2 | 95.3 | 7.3<br>R = –0.25; p = 0.86 | 27.0<br>R = 1.00; p < 0.01 | 30.6<br>R = 0.97; p < 0.02 |
| Euglenophyceae | 2 | 89.3 | 23.2<br>R = 0.65; p < 0.03 | 7.8<br>R = 0.20; p = 0.18 | 49.8<br>R = 1.00; p < 0.02 |
| Xanthophyceae | 1 | N/A | 19.6 | 9.7 | 46.2 |
| Cryptophyceae | 1 | N/A | 19.7 | 47.9 | 12.7 |

contributors via Fourier-transformed pattern recognition (Oldham et al. 1985), discriminant analysis (Johnsen et al. 1994), similarity indices (Millie et al. 1997, 2002; Staehr and Cullen 2003) that are based on 4th-derivative transformations (Butler and Hopkins 1970a, b), principal components analysis (Moberg et al. 2002; Seppälä and Olli 2008), Gaussian decomposition of the spectra (Bodemer 2004; Chekalyuk and Hafez 2008) or linear unmixing (Dickinson et al. 2001; Beutler et al. 2002; Beutler et al. 2003; Beutler et al. 2004; Gaevsky et al. 2005; Parésys et al. 2005; Zhang et al. 2006; Seppälä and Olli 2008). The last is the most widely-used approach and is the method implemented in commercial instruments manufactured by Walz and *bbe* Moldaenke. The basis is that the fluorescence of an unknown sample at a wavelength $x$ is the sum of the contributions of $n$ known groups. The contribution of each group is equal to its concentration, as Chl*a*, and its Chl*a*-specific fluorescence (Eq. 1):

$$Fl(\lambda_x) = \sum_{n=1}^{n=i} Fl^{Chl}(\lambda_x)_n \bullet Chl_n \qquad (2)$$

The spectral fluorescence signature, SFS, which comprises the signals at multiple wavelengths ($x_1$, $x_{2...}$ $x_m$), is then defined in terms of three matrices (Seppälä and Olli 2008):

$$SFS = CF + E \qquad (3)$$

where $SFS$ is a matrix of y sample spectra ($y$ by $x$), $C$ is a matrix of the Chl*a* concentrations of the known taxa ($y$ by $n$), $F$ is a matrix of the Chl*a*-specific fluorescence intensities of the known taxa ($x$ by $n$), and $E$ is an error matrix. In the case of ambiguity or mutual exclusion between similar taxa in the solution, the approach can be qualified with a decision-tree (Parésys et al. 2005). Here, one or more criteria are used to select alternative sets of $C$ and $F$ matrices (e.g. for distinguishing between PE-rich and PC-rich cyanobacteria, in the case where one or the other dominates).

Figure 5 illustrates linear unmixing, using Chl*a* fluorescence excited by LEDs in five wave-bands. The SFS of the four known taxa are shown normalized to the mean value, as Norm SFS, in Fig. 5a. Differences in the Norm SFS can be attributed to differences in pigment complements. The representative cyanobacterium, *Synechococcus bacillaris*, is PC- rather than PE-rich, so its SFS is dominated by the excitation spectrum of PC

(Fig. 1). The Norm SFS of the representative diatom, chlorophyte and cryptophyte are more similar to each other than to the cyanobacterium, reflecting differences in the distribution of pigments between eukaryotes vs procaryotes (see above) and differ from each other primarily in their relative magnitudes at 470–570 nm. This is the region of the spectrum that is most sensitive to the presence and abundance of photosynthetic carotenoids (the diatom), phycoerythrin (the cryptophyte) or their absence (the chlorophyte). The Norm SFS of two "unknowns", the diatom *Entomoneis* cf. *alata* and the unicellular rhodophyte *Porphyridium cruentum*, are shown in Fig. 5b. Note the similarity between *Entomoneis'* Norm SFS and those of the known diatom, the cryptophyte, and the chlorophyte. The Norm SFS for the second unknown, *Porphyridium*, is not obviously similar to any of four known taxa.

The similarity matrix is represented in an MDS plot (Fig. 5c), where the four known Norm SFS define each apex of a tetrahedron. The lines joining any two points represent binary mixtures of those two taxa. The planes defined between any three points represent ternary mixtures of the three. The internal volume of the tetrahedron represents all quarternary mixtures for positive solutions of Eq. 3. The solution to Eq. 3 for *Entomoneis* is a binary mixture of the representative diatom, *Thalassiosira pseudonana*, (65%) and the cryptophyte, *Rhodomonas lens*, (35%) as shown by its position on the line connecting their SFS (Fig. 5c). In contrast, ordination of *Porphyridium* Norm SFS on the MDS plot places it outside the tetrahedron of positive solutions to Eq. 3, and closest to the cryptophyte and the representative cyanobacterium, *Synechococcus bacillaris* (Fig. 5c). Intuitively, this makes sense: the rhodophyte, like the cyanobacterium, has a phycobilisome and lacks Chl*c* and PSC, so would have a relatively low contribution from them at 470–525 nm (Figs. 1 and 5b). However, unlike this cyanobacterium, but like the cryptophyte, it is PE-rich, resulting in high excitation at 525 nm (Fig. 5b). Because the fit lies outside the region of positive fits to the four Norm SFS, it must be constrained to

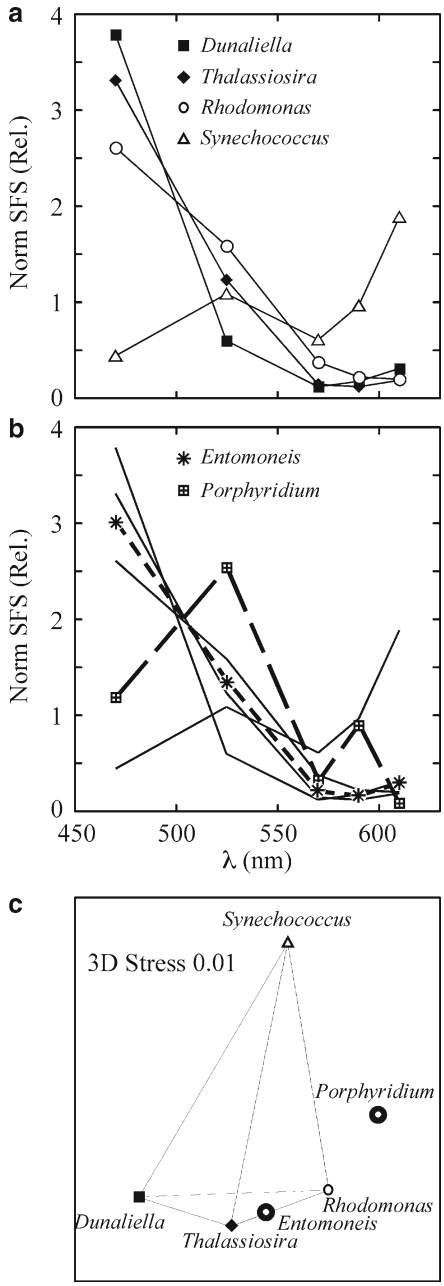


**Fig. 5** (continued) signatures from (a), which are shown as fine lines. (**c**) Multidimensional scaling plot (MDS) of the calibration signatures from (**a**) and the unknown signatures from (**b**). The lines connecting each pair of calibration signatures represents the mixing line of two-component mixtures (see text for details)

**Fig. 5** (**a**) Normalized spectral fluorescence-excitation signatures (Norm SFS) for nutrient-replete cultures of a representative chlorophyte (*Dunaliella tertiolecta* CCMP1320), chromophyte (the diatom *Thalassiosira pseudonana* CCMP1335), cryptophyte (*Rhodomonas lens* CCMP739) and cyanobacteriaum (*Synechococcus bacillaris* CCMP1333). The spectra were collected with *bbe* Moldaenke's Algae Online Analyzer (AOA), corrected according to Kopf and Heinz (1984) and normalized to the average of the weighting coefficients to emphasize differences in shape. (**b**) Normalized SFS for a second diatom (*Entomoneis cf alata* CCMP1522) and a unicellular rhodophyte (*Porphyridium cruentum* CCMP1328). These are superimposed on the calibration

positive contributions, which translates to a mixture of the cyanobacterium (24%) and the cryptophyte (76%).

Three assumptions must be met for accurate identification with linear unmixing, (Beutler et al. 2002):

1. The signatures of the known taxa must be linearly independent so that it is not possible to reproduce the signature of one taxon by the weighted sum of the others.
2. The signatures of the known groups must be invariant (i.e. the terms on the right-hand side of Eq. 1 must be constant or must have compensatory changes, so that $Fl^{Chl}(\lambda)$ is constant).
3. The spectral fluorescence signatures must be determined with sufficient accuracy.

The first assumption has been validated by Beutler and co-workers (2002), for an instrument using five excitation wavelengths and a single detection wavelength in what are now commercially-available configurations, *bbe* Moldaenke's Fluoroprobe and Algae Online Analyzer (Fig. 5). Note that assumption (1) must be tested for any different configuration when using other wavelengths for excitation and/or emission. We present data to evaluate assumptions (2) and (3) below, using the Algae Online Analyzer (AOA). The instrument can be trained on up to five SFS without being underconstrained but we focused on the four characteristic of our local estuarine waters, PC-rich cyanobacteria, chlorophytes, cryptophytes and chromophytes.

## 3 Variation in Chlorophyll-specific Fluorescence, $F^{Chl}$

It became clear very soon after the introduction of the *in vivo* fluorescence as an estimate of Chl*a*, (Lorenzen 1966), that the ratio of fluorescence to Chl*a* ($Fl^{Chl}$) is not constant. The ratio was shown to vary between species (Strickland 1968; Loftus and Seliger 1975), with light exposure and nutrient availability (Kiefer 1973a, b; Loftus and Seliger 1975; Vincent 1979), and with cell size (Alpine and Cloern 1985). For recent reviews, see Babin (2008) and Chapter 3. The observation of variable $Fl^{Chl}$ has been reiterated frequently in the decades since (e.g. Kruskopf and Flynn 2006) and has been explicitly recognized by almost all researchers working on the use of SFS-based taxonomy since Yentsch and Yentsch (1979). Strictly, this invalidates Assumption (2), above. In addition to the effect that variability in $Fl^{Chl}$ has on the estimate of Chl*a* concentration, changes in the spectral dependence of $Fl^{Chl}$ will result in mis-identification through linear unmixing where a single representative signature is used for each taxon.

### 3.1 Inter-Specific Variability

We illustrate the effect of inter-specific variability (cf. the data of Gaevsky et al., Fig. 4) on estimates of taxonomic composition and abundance in Fig. 6. The AOA was calibrated with one representative of each of the chlorophytes, chromophytes (diatom), cryptophytes and cyanobacteria (Fig. 5) and then challenged with 11 chromophytes from four classes. All cultures were nutrient-replete and grown at the same irradiance in semi-continuous culture (MacIntyre and Cullen 2005). Comparison of the Norm SFS of the chromophytes with those of the calibration species showed that they clustered with the representative chromophyte but did show significant dispersion (Fig. 6a). The similarity comparisons between the unknown chromophytes and calibration representative, *Thalassiosira pseudonana*, (not shown) were higher than between the unknowns and the other calibration taxa and higher than between *T. pseudonana* and the other calibration taxa. In short, as shown with the data of Gaevsky and coworkers (Fig. 4, Table 1), the classification of SFS followed the unknown species' taxonomic affiliation. Because this comparison is based on normalized signatures (i.e., the shape of the SFS alone), it reflects differences in the spectral dependence of excitation arising from differences in $a_{PS}^{Chl}(\lambda_{Ex})$ and $\phi(\lambda_{Ex,Em})$ in Eq. 1. These in turn reflect differences in the ratio of pigments, the internal concentration of pigments and the degree of pigment packaging, the quantum yield of photosynthesis, and the likelihood of excess energy being re-emitted as fluorescence rather than directed into other dissipative pathways.

When linear unmixing is used to estimate the taxonomic composition, the monocultures were identified as dominated by chromophytes, with lesser contributions from the 3 other groups. In all but one case, the component of the population that was mis-identified was attributed to chlorophytes or cryptophyes (Fig. 6b), reflecting the proximity of the unidentified species'

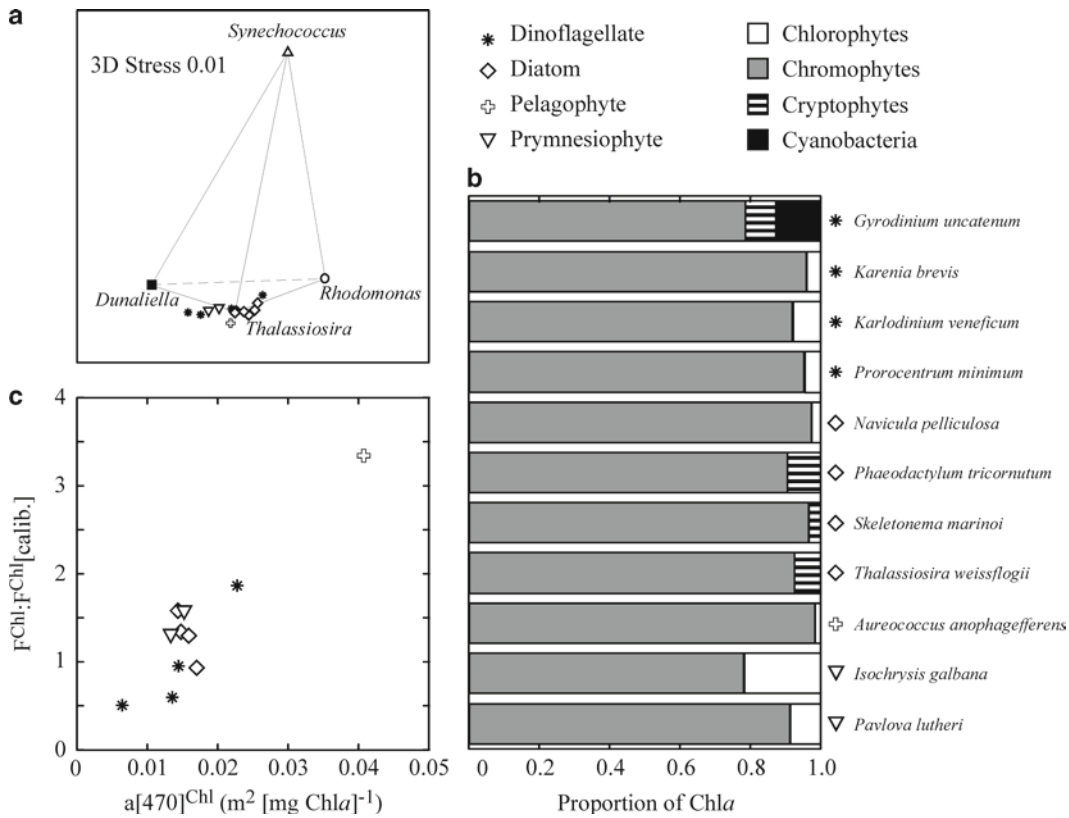


**Fig. 6** (**a**) Multidimensional scaling plot (MDS) of the AOA's calibration signatures from Fig. 5c and the signatures of 11 'unknown' chromophytes (dinoflagellates, diatoms, prymnesiophytes and a pelagophyte). The unknown chromophytes clustered most closely with the calibration chromophyte (the diatom *Thalassiosira pseudonana*) but, as indicated by the dispersion in the MDS, were not identical. (**b**) The AOA's classification of the 11 unknown chromophytes, based on linear unmixing fits to the calibration SFS (Fig. 5a). Because of the variance in their SFS (cf. Fig. 5b), they were identified as being 79–98% chromophytes, with 2–21% contributions of other taxa. (**c**) $F^{Chl}$ at 470 nm for the 11 unknown chromophytes, expressed as the ratio to $F^{Chl}$ of the calibration chromophyte, as a function of Chl*a*-specific absorption at 470 nm

Norm SFS to the eukaryote mixing plane (the chlorophyte-chromophyte-cryptophyte surface, Fig. 6a). Differences between the SFS of the three eukaryotes used to calibrate the AOA are driven primarily by changes in the ratio of PSC or PE to accessory chlorophylls (Figs. 1 and 5a). The estimates of relative abundance (Fig. 6), which ranged from 79–98% chromophytes and 2–21% other taxa, depend on both the shape of the signature (the norm SFS) and each of the 4 calibration species' spectrally-weighted values of $Fl^{Chl}$ (Eq. 2). The low $Fl^{Chl}$ of the calibration cyanobacterium relative to the eukaryotes (0.05–0.13$x$ of the eukaryotes' values at 470 nm, and 0.33–1.67$x$ at 525 nm), is the reason that a relatively minor deviation from the eukaryote mixing plane towards the cyanobacterial apex can result in a disproportionate apparent contribution by the cyanobacteria. This is illustrated by the 12% contribution of cyanobacteria to the estimated composition of the dinoflagellate *Gyrodinium uncatenum* (Fig. 6b), although its SFS, which is the right-most of the unknown chromophytes' (Fig. 6a), is little further from the eukaryotes' mixing plane than those of the adjacent diatoms.

The degree to which the linear unmixing over- or under-estimates the chlorophyll concentration of the unknown samples depends on the relative magnitude of $Fl^{Chl}$ for each species (Eq. 2). This in turn reflects the Chl*a*-specific photosynthetic cross-section, $a_{PS}^{Chl}$, which depends on both the relative abundance of photosynthetic vs photoprotective pigments and the degree of pigment packaging. The importance of the latter is illustrated in Fig. 6c, which shows the variation in $Fl^{Chl}$

as a function of Chl*a*-specific absorption at 470 nm. The values of $a(470)^{Chl}$ decrease by 6.4*x* between the smallest cell, *Aureococcus anophagefferens* (c. 1.5 µm) and the largest, *Gyrodinium uncatenum* (c. 45 x 60 µm) as pigment packaging (internal self-shading) increases. The residual variation in $Fl^{Chl}$ reflects differences in the relative abundance of photosynthetic vs photoprotective pigments and the effective quantum yield of fluorescence ($a_{PS}^{Chl}$ vs $a^{Chl}$ and $\phi(\lambda_{Ex,Em})$, Eq. 1). The same pattern holds for the other 4 wavelengths used by the AOA.

## 3.2 Intra-specific Variability

Intra-specific variability in photosynthetic architecture (the constituents of the photosynthetic apparatus) occurs in response to variability in nutrient availability (Laws and Bannister 1980; Kolber et al. 1988; Sosik and Mitchell 1991), temperature (Verity 1981; Sosik and Mitchell 1994; Moore et al. 1995; Anning et al. 2001) and irradiance (reviewed by MacIntyre et al. 2002). The effect on $Fl^{Chl}$ of acclimation to changing light intensity and nutrient availability in the diatom *Thalassiosira pseudonana* are illustrated in Fig. 7. There is relatively little variation in either the quantum yield of PSII activity or $Fl^{Chl}$ for nutrient-replete cultures of *Thalassiosira pseudonana* (Fig. 7a, b): coefficients of variation are 2% and 15%, respectively. The quantum yield of PSII activity is determined here with DCMU (3-[3,4-dichlorophenyl]-1,1-dimethylurea) and is termed cellular fluorescence capacity, CFC (Vincent 1980), to distinguish it from the analog that is measured using PAM or FRR fluorescence, $F_v/F_m$. Under nutrient-limited growth (i.e., when cultures are in balanced growth and fully acclimated to reduced nutrient availability in chemostats, MacIntyre and Cullen 2005),

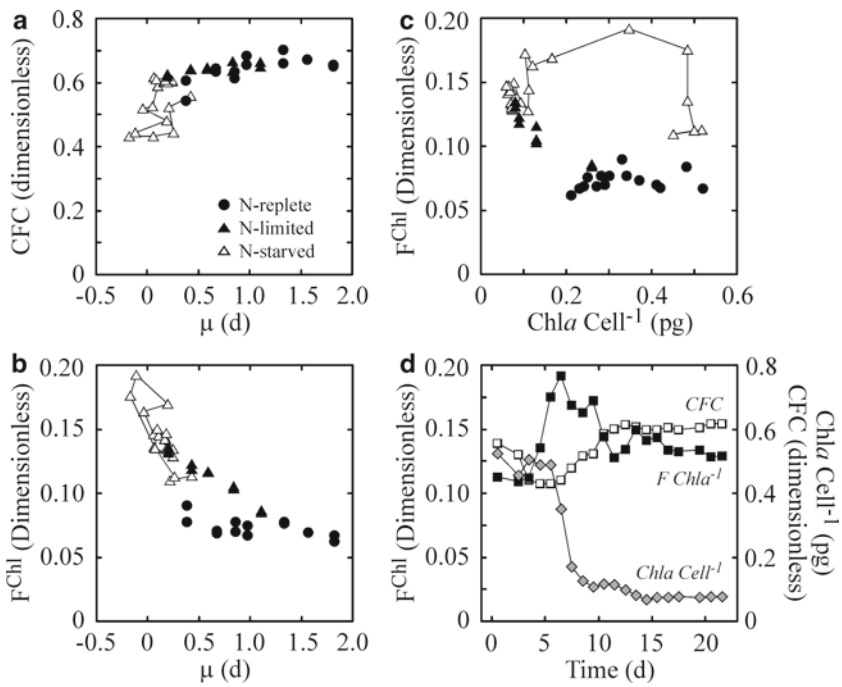


**Fig. 7** Variation in (**a**) quantum yield of PSII activity (CFC) and (**b**) $F^{Chl}$ in the diatom *Thalassiosira pseudonana* as a function of growth rate in balanced (N-replete and N-limited) and unbalanced (N-starved) growth. Data for the N-starved culture represent the trajectory through acclimation to N-limitation (see **d**). $F^{Chl}$ is parameterized as the dimensionless ratio of fluorescence *in vivo* to fluorescence *in vitro* (Kiefer 1973a). (**c**) Variation in $F^{Chl}$ with pigment quota in the same samples. (**d**) Time-course of CFC, $F^{Chl}$ and pigment quota during acclimation to N-limitation after an exponential-phase batch culture was switched to chemostat mode (see text for details). Data of Yang, MacIntyre and Cullen, reported in part by Cullen and co-workers (Cullen et al. 1992; Zhu et al. 1992; Parkhill et al. 2001; MacIntyre et al. 2002; MacIntyre and Cullen 2005). Panel (**d**) is based on figures from MacIntyre and Cullen (2005)

$Fl^{Chl}$ is correlated with the degree of nutrient limitation, expressed as the reduction in growth rate in the chemostats. There is a significant ($p < 0.01$) but relatively minor reduction in CFC: a 5% decline over an 82% reduction in growth rate, as compared to a 53% increase in $Fl^{Chl}$. These trends may be over-estimates of the true variability, due to an actinic effect of the excitation beam in the fluorometer causing some photosynthetic induction (Parkhill et al. 2001).

Although down-regulation of pigments occurs under both high irradiance and low nutrient availability (Geider et al. 1997, 1998a, b), the reduction in pigment, on a per-cell or per-carbon basis, is more pronounced over the range of nutrient limitation than over the range of nutrient-replete growth. The increase in $Fl^{Chl}$ is significantly correlated with the reduction in pigmentation ($p < 0.001$; $R = -0.93$: Fig. 7c), suggesting that an increased Chl*a*-specific efficiency of light harvesting through reduction of the package effect is largely responsible for the increase (cf. Fig. 6c). (We note that the inverse relationship between these variables could be a spurious correlation (Jackson and Somers 1991), driven by the presence of chlorophyll concentration in both variables. However the quotient $F\ Cell^{-1}$ for N-limited cultures has a higher range than does chlorophyll concentration, 5.0*x* vs 2.7*x*, indicating that the relationship is robust.)

While variation in $Fl^{Chl}$ and CFC under N-limitation (balanced growth) is modest, the range under nutrient starvation (unbalanced growth) is less so. Fig. 7d shows the response of a batch culture in late exponential phase having severe limiting nutrient supply imposed on it by being switched to chemostat mode (see MacIntyre and Cullen 2005, for details). The nutrient supply was at 0.15 of the nutrient-replete growth rate. In the initial phase of nutrient-starvation, there is a rapid reduction in CFC and a corresponding rise in $Fl^{Chl}$. Given that CFC is correlated with the maximum quantum yield of photosynthesis, a reduction in CFC reflects a reduced efficiency of energy transfer into photosynthesis, which will lead to a compensatory increase in energy dissipation as fluorescence or heat. The initial phase of nutrient starvation is succeeded by an acclimative down-regulation of Chl*a* (Fig. 7d) during resource re-allocation to balance light harvesting and growth (Geider et al. 1998a). After the initial very rapid phase of down-regulation, both CFC and $Fl^{Chl}$ recover and all three eventually reach the new equilibrium condition of balanced, nutrient-limited growth. The trajectories of both CFC and $Fl^{Chl}$ through the transition from nutrient starvation to nutrient limitation are superimposed on the data for acclimated cultures (Fig. 7a–c). Two observations are obvious. First, the range of values falls well outside the envelope of responses for cultures in balanced growth. The range in $Fl^{Chl}$ is 42% higher than the maximum observed under extreme nutrient limitation (growth at 15% of the nutrient-replete growth rate at an irradiance $1.75x\ K_E$, the irradiance at which nutrient-replete growth becomes light-saturated). The second observation is that $Fl^{Chl}$ does not covary with pigment quota and pigment packaging during nutrient starvation (Fig. 7c), in contrast to both the inter- and intra-specific trends for acclimated cultures (Fig. 6c, 7c). We can infer that variability in $Fl^{Chl}$ (Eq. 1) is driven primarily by variability in $a_{PS}^{Chl}(\lambda_{Ex})$ in balanced growth but must also be driven by variability in $\phi(\lambda_{Ex,Em})$ in unbalanced growth.

The intra-specific variability in $Fl^{Chl}$ shown in Fig. 7 is for data collected at a single wavelength. Given the relationship between $Fl^{Chl}$ and the estimate of Chl*a* (Eq. 2), we would predict that fluorescence-based estimates of biomass will be biased by variation in $Fl^{Chl}$ resulting from changes in photosynthetic architecture and efficiency (Fig. 6c, 7c). The prediction is borne out by repeated observation of variability in the relationship between fluorescence and Chl*a* over the past 30 years (see above). It is difficult to predict if the taxonomic classification based on SFS will be as sensitive. Accurate identification depends on invariant spectral signatures, which in turn depend on constant ratios of functional pigment arrays. What constitutes a functional array depends on the interrogation wavelengths. If accessory pigments and Chl*a* are both excited, then the ratios of accessory pigments to Chl*a* will determine the constancy of the SFS (or the lack of constancy). However, for instruments that target only the accessory pigments (e.g. the AOA: compare the excitation wavelengths in Fig. 5a with the absorption spectra in Fig. 1), then the critical ratios will be the abundances of accessory chlorophylls, photosynthetic carotenoids and phycobilins relative to each other.

Studies of chromophytes growing under nutrient-replete conditions show relatively little variation in the ratios of Chl*c* and PSC to Chl*a* when growing below $K_E$ (reviewed by MacIntyre et al. 2002). At irradiances above $K_E$, there is a selective loss of both Chl*c* and PSC relative to Chl*a*. However, ratios of PSC to Chl*c* are more constrained than the ratios of either to Chl*a* (Table 2). In all cases, the ratios of PPC to photosynthetic pigments have a wide range, increasing with irradiance. There are few reports of pigments in

**Table 2** Variations in pigment ratios (g $g^{-1}$) for cells in nutrient-replete growth over a range of irradiances. The irradiance range is expressed relative to the saturating irradiance for growth ($E/K_E$ – see MacIntyre et al. 2002). Data are for the chromophytes *Thalassiosira weissflogii* (diatom), *Amphidinium carteri* (dinoflagellate), *Emiliania huxleyi, Hymenomonas carterae* and *Phaeocystis antartica* (prymnesiophytes) and the cyanobacterium *Synechococcus* sp. (clones WH7803). PB is the sum of PE and PC

| Species & Source | $E/K_E$ | Chl*c*: Chl*a* | PSC: Chl*a* | PE:Chla | PC:Chla | PPC: Chl*a* | PSC: Chl*c* | PPC: Chl*c* | PSC: PPC | PB:PPC |
|---|---|---|---|---|---|---|---|---|---|---|
| *Thalassiosira weissflogii* (Sosik 1988) | 0.1–10.3 (79x) | 0.6–1.0 (1.7x) | 0.34–0.37 (1.1x) | N/A | N/A | 0.05–0.29 (5.8x) | 0.37–0.57 (1.5x) | 0.05–0.46 (9x) | 1.2– .0 (5.7x) | N/A |
| *Thalassiosira weissflogii* (Goericke and Welschmeyer, 1992a, b) | 0.2–10.1 (51x) | 0.4–1.0 (2.8x) | 0.25–0.37 (1.5x) | N/A | N/A | 0.06–0.40 (6.7x) | 0.29–1.0 (3.6x) | 0.06–1.12 (19x) | 0.9–5.3 (5.8x) | N/A |
| *Amphidinium carteri* (Sosik 1988) | 0.7–9.5 (14x) | 0.8–1.0 (1.2x) | 0.60–0.68 (1.1x) | N/A | N/A | 0.15–0.39 (2.6x) | 0.61–0.80 (1.3x) | 0.15–0.46 (3.1x) | 1.7–4.2 (2.4x) | N/A |
| *Emiliania huxleyi* (Stolte et al. 2000) | 0.2–7.8 (34x) | 0.5–1.0 (2.0x) | 0.6–1.2 (1.9x) | N/A | N/A | 0.1–0.8 (5.6x) | 1.1–1.3 (1.2x) | 0.2–1.6 (10x) | 0.8–8.2 (10x) | N/A |
| *Hymenomonas carterae* (Sosik 1988) | 0.14–8.5 (61x) | 0.8–1.0 (1.3x) | 0.28–0.36 (1.3x) | N/A | N/A | 0.08–0.26 (3.3x) | 0.34–0.42 (1.2x) | 0.10–0.32 (3.2x) | 1.1–4.3 (4.0x) | N/A |
| *Phaeocystis antarctica* (Moisan and Mitchell 1999) | 0.2–6.2 (39x) | 0.4–1.0 (2.3x) | 0.3–0.7 (2.4x) | N/A | N/A | 0.02–0.4 (19x) | 0.4–0.7 (1.9x) | 0.02–0.9 (43x) | 0.8–8.2 (57x) | N/A |
| *Synechococcus sp.* WH7803 (Kana and Glibert 1987; Kana et al. 1988) | 0.3–13.8 (44x) | N/A | N/A | 4.4–38.6 (8.8x) | 1.5–2.7 (1.8x) | 0.55 – 1.6 (2.8x) | N/A | N/A | N/A | 0.01–0.24 (17x) |

chlorophytes grown over comparable ranges of irradiance but the Chl*b*:Chl*a* ratio in *Dunaliella tertiolecta* and *D. salina* varies about 2*x* (Sukenik et al. 1990; Neidhardt et al. 1998) over a 24*x* range in growth irradiance. It varies 3.3*x* in the Chl*b*-containing cyanobacterium *Prochlorococcus marinus* (Moore et al. 1995) grown at 0.5–15.0 $E/K_E$. There is a preferential loss of phycobilins relative to Chl*a* with increasing irradiance in nutrient-replete cryptophytes (Lewitus and Caron 1990; Sciandra et al. 2000; Hammer et al. 2002) and cyanobacteria (Table 2) and a preferential loss of PE over PC in the latter (Kana and Glibert 1987; Six et al. 2004). The losses in cyanobacteria reflect the progressive shortening of the phycobilin rods in the phycobilisome vs the stable Chl*a*-containing reaction center (Grossman et al. 1993). There are comparable or greater changes in pigment ratios under both nutrient-limitation and nutrient-starvation in representatives of the chromophytes, crytophytes and cyanobacteria (Collier et al. 1993; Latasa and Berdalet 1994; Latasa 1995; Goericke and Montoya 1998; Sciandra et al. 2000; Henriksen et al. 2002; Staehr et al. 2002). In contrast, there was only 1.1*x* variability in Chl*b*:Chl*a* under a 9*x* range of nutrient-limited growth rates in the chlorophyte *D. tertiolecta* (Sosik and Mitchell 1991), as compared to the c. 2*x* range when grown over a 24*x* range of irradiance (Sukenik et al. 1987).

Assessing the effect of changing pigment quotas on taxonomic classification requires knowledge of whether the change makes them more or less like members of other taxonomic groups. This depends on both the magnitude/type of change in the pigment ratios and on the wavelengths at which the SFS are determined. We tested the effect of simultaneous nutrient starvation and increased irradiance (both of which drive down-regulation of pigments) on the four calibration species (Fig. 5), using the AOA. Nutrient-replete cultures in mid- to late-exponential phase were subject to a 10% daily dilution with N-free medium and monitored for biochemical composition and their taxonomic signatures. Nitrate was exhausted within 6 days in all cultures and Chl*a* concentrations declined as the growth rate declined below the dilution rate and the cells underwent washout (Fig. 8a–d). This raised the effective irradiance in the 10-L (0.22 m diameter) culture vessels so that the cultures were subject to the synergistic effects of reduced nutrients and increased irradiance on regulation of light harvesting. In all cases, the increase in C:N and decrease in Chl*a*:C ratios (Fig. 8e–h) indicated progressive down-regulation of light harvesting, although the time-courses differed between species. There were only minor changes in accessory chlorophyll:Chl*a* ratios in the eukaryotes (Fig. 8i–k) and a minor increase in photosynthetic carotenoid:Chl*a* ratios in the diatom *Thalassiosira pseudonana* (Fig. 8j). Estimates of phycobilins from whole-cell absorption indicated an initial increase as cells continued to grow, followed by a decrease during the combined nutrient-stress and increased irradiance, in both the cryptophyte *Rhodomonas lens* and the cyanobacterium *Syncechococcus bacillaris* (Fig. 8k–l). In all cases, the PPC:Chl*a* ratio increased (Fig. 8i–l). These changes were easily visible as the cultures turned from deep green (the chlorophyte *Dunaliella tertiolecta*), pink (*Rhodomonas*) or blue-green (*Synechococcus*) to yellow-green or from brown to orange-brown (*Thalassiosira*).

The changes in pigment ratios were reflected in the Norm SFS (Fig. 9a-d). In *Dunaliella*, there was a minor steepening of the decrease between 470 and 525 nm, presumably as a consequence of increased masking of Chl*b*'s absorption by lutein (Fig. 8i) and/or β-carotene (which was not quantified). In *Thalassiosira*, the Norm SFS were effectively invariant (Fig. 9b). As with *Dunaliella, Rhodomonas* showed a progressive steepening of the Norm SFS between 470 and 570 nm (Fig. 9c), reflecting both the progressive loss of PE and the increase in alloxanthin (Fig. 8k) and/or β-carotene relative to Chl*a* and Chl*c*. In *Synechococcus*, the Norm SFS were driven by the changes in PC:Chl*a* (Fig. 8l), with the peaks at 525 and 610 nm becoming more pronounced as the ratio increased and then progressively flatter as it fell again. The high variation at 470 nm in the Norm SFS (Fig. 9d) is largely an artifact of normalization: the change in $F^{Chl}$ at 610 nm was 27*x* that at 470 nm, so normalizing to the mean $F^{Chl}$ across wavelengths resulted in the values at all wavelengths being driven by variability at 610 and, to a lesser extent, 570 and 590 nm.

The matrix of the pair-wise similarity coefficients is displayed in an MDS plot (Fig. 9e), in which the varying Norm SFS are compared with the apices of the tetrahedron formed by the Norm SFS of the cultures used for the calibration. Because the chlorophyte already has the steepest decline in Norm SFS of the eukaryotes (Fig. 5a), the progressive steeping of the Norm SFS makes the nutrient-starved cultures less, rather than more, like the other eukaryotes. In the calibration, the

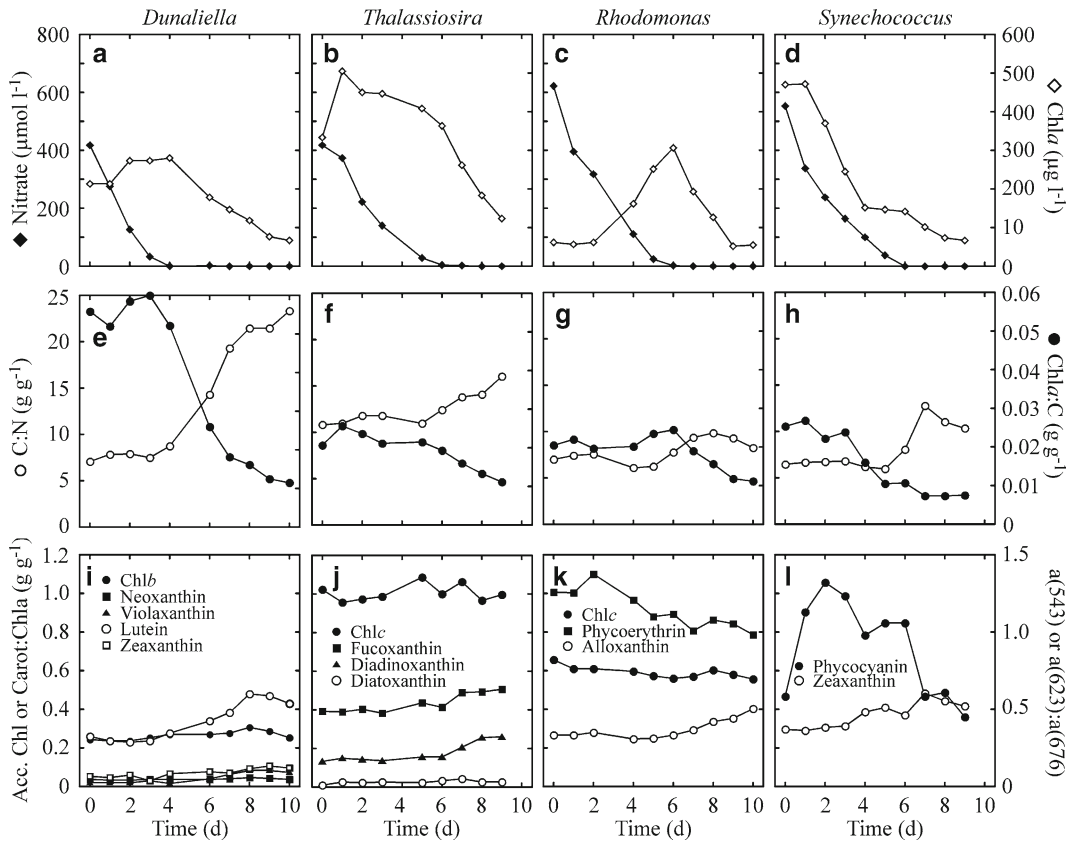


**Fig. 8** Time-courses of (**a-d**) nitrate drawdown and biomass (as Chl*a*); (**e–h**) C:N and Chl*a*:C; and (**i–l**) pigment:Chl*a* ratios in the chlorophyte *Dunaliella tertiolecta* (A, E and I), the chromophyte (diatom) *Thalassiosira pseudonana* (B, F and J), the cryptophyte *Rhodomonas lens* (C, G and K), and the cyanobacterium *Synechococcus bacillaris* (D, H and L). Mid- to late-exponential phase cultures were diluted 10% daily with N-free medium. Chlorophylls and carotenoids were determined by HPLC. Concentrations of β-carotene were not determined. Phycobilins are approximated as the ratio of peak absorption (543 and 623 nm) to absorption at the Chl*a* red peak (676 nm) *in vivo*

cryptophyte has the most gradual decline in Norm SFS between 470 and 570 nm (Fig. 5a). Consequently, the progressive steepening caused by selective loss of PE, in the absence of photosynthetic carotenoids, makes it more like the chlorophyte: note that the change lies very close to the cryptophyte-chlorophyte mixing line (Fig. 9e). The largely invariant Norm SFS of the chromophyte is evident from the minimal dispersion between samples. Last, the initial increase in PC:Chl*a* in the cyanobacterium (Fig. 8l) was manifested as more pronounced peaks at 525 and 570–610 nm. These are less, not more, similar to the Norm SFS of the eukaryotes (Fig. 5a), causing the initial move away from their mixing plane (Fig. 9e). The subsequent loss of PE, again in the absence of photosynthetic carotenoids, also resulted in the cyanobacterium's Norm SFS becoming more like the chlorophyte's, as evidenced from their proximity to the cyanobacterium-chlorophyte mixing line (Fig. 9e).

The changes in Norm SFS caused negligible inaccuracies in taxonomic classification in the chlorophyte and chromophyte (Fig. 10a, b). Because their Norm SFS became increasingly similar to that of the calibration chlorophyte (Fig. 9e), both the cyanobacterium and, particularly, the cryptophyte had progressive inaccuracies in taxonomic classification. In both, linear unmixing of the SFS converged on a mixture of the correct taxon and chlorophytes (Fig. 10c, d). As predicted, $Fl^{Chl}$ increased

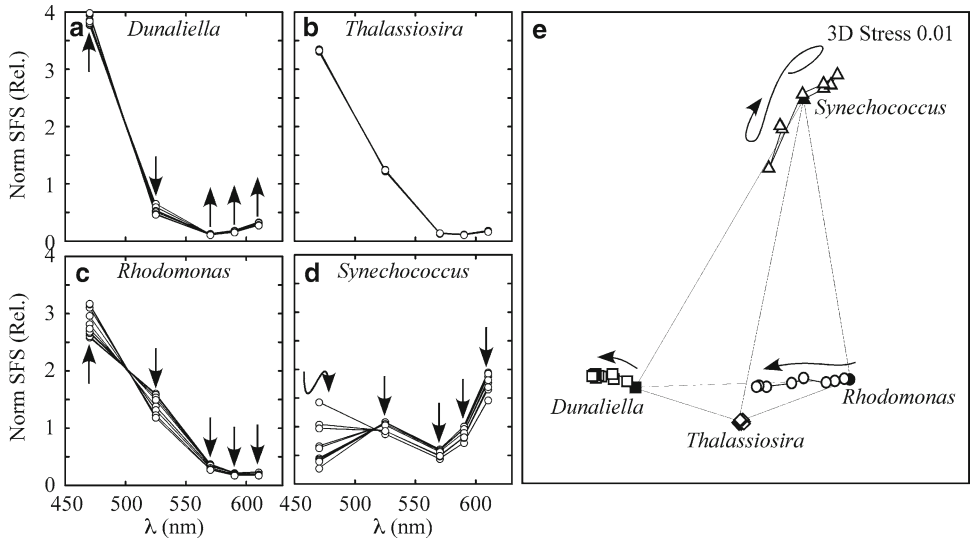


**Fig. 9** Changes in the Norm SFS for (**a**) the chlorophyte *Dunaliella tertiolecta,* (**b**) the chromophyte (diatom) *Thalassiosira pseudonana,* (**c**) the cryptophyte *Rhodomonas lens* and (**d**) the cyanobacterium *Synechococcus bacillaris* under progressive N- and light-stress (see text for details). Arrows denote the net direction of change over the time-course at each wavelength. (**e**) Multidimensional scaling plot of the Norm SFS from A-D (open symbols) superimposed on the calibration signatures (closed symbols, cf. Fig. 5c). Arrows denote the time-course

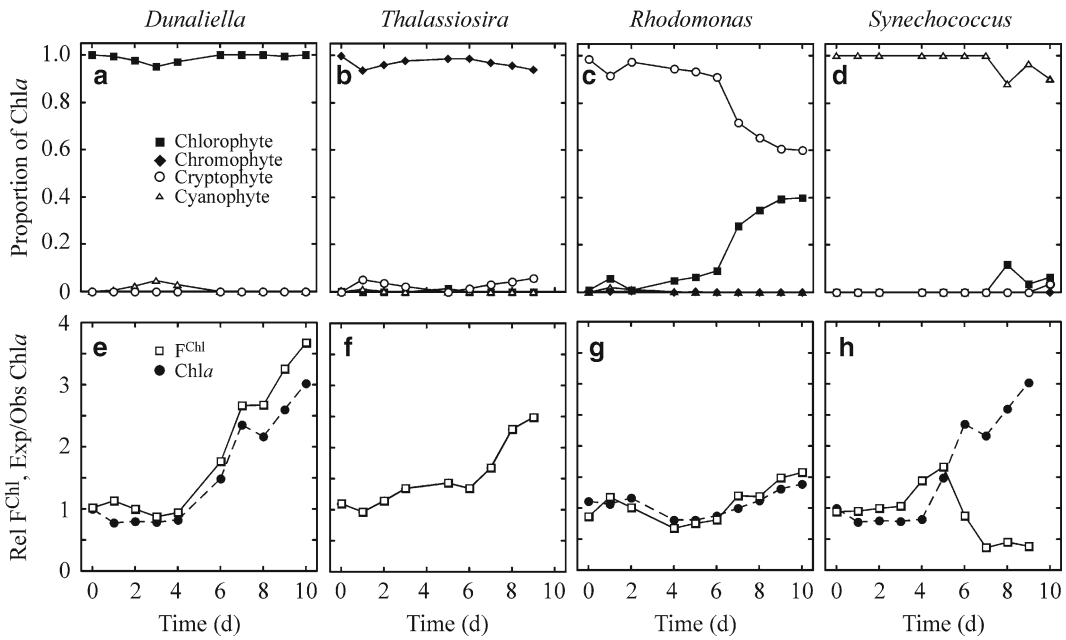


**Fig. 10** Time-courses of (**a-d**) taxonomic classification (as the proportion of total Chl*a*); and (**e–h**) relative $F^{Chl}$ and estimated Chl*a* in the chlorophyte *Dunaliella tertiolecta* (**a** and **e**), the chromophyte (diatom) *Thalassiosira pseudonana* (**b** and **f**), the cryptophyte *Rhodomonas lens* (**c** and **g**), and the cyanobacterium *Synechococcus bacillaris* (**d** and **h**) under progressive N- and light-stress (see text for details). Taxonomic classification is the output of the linear unmixing solution to the fluorescence signature. Values of $F^{Chl}$ are at the peak wavelength (470 nm for the eukaryotes and 610 nm for the cyanobacterium) and are expressed as ratios to the calibration values. Chl*a* is expressed as the ratio of the value predicted from the linear unmixing to the value determined by HPLC

at all wavelengths, which was reflected in over-estimates of Chl*a* by up to 3*x* (Fig. 10e–h). The over-estimate of Chl*a* in the cyanobacterium (*Synechococcus*, Fig. 10h) was caused by the mis-assigned classification and the taxonomic differences in $F^{Chl}$.

### 3.3 Short-Term Quenching

So far, we have considered only the effects of relatively slow changes in photosynthetic architecture, involving regulation of pigment quota, on SFS. Other changes that might also affect SFS are much more rapid (MacIntyre et al. 2000). Short-term variation in $Fl^{Chl}$ reflects the balance between light harvesting and downstream utilization of reductant, which is the basis of efforts to estimate photosynthetic rates from variable fluorescence (Falkowski et al. 1988; Genty et al. 1989; 1990; Krause and Weis 1991), discussed by Suggett, Moore and Geider in Chapter 5 (see also Suggett et al. 2009). The magnitude of $Fl^{Chl}$ depends both on the balance between the activities of photosynthetic and dissipative pathways within the photosynthetic apparatus and on the intensity and duration of the excitation (reviewed by Kromkamp and Forster 2003). This is illustrated in Fig. 11a, which shows fluorescence measured before ($F_0$, $F$) and after ($F_m$, $F_m'$) the application

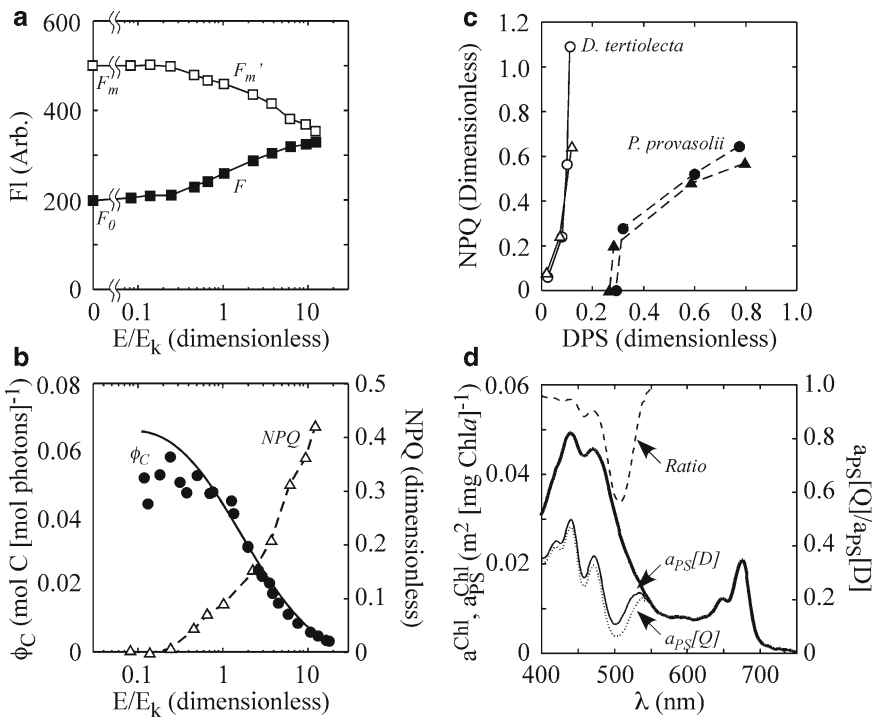


**Fig. 11** (**a**) Minimum ($F_0$ and $F$) and maximum ($F_m$ and $F_m'$) fluorescence in darkness ($F_0$, $F_m$) and with actinic illumination ($F$, $F_m'$) in the prasinophyte *Pycnococcus provasolii*. Fluorescence was measured with a Walz PAM101. Background irradiance is expressed in terms of the saturating parameter of a parallel $^{14}$C photosynthesis-irradiance (PE) curve, $E_k$, after reconciliation for differences in light quality (MacIntyre and Cullen 2005). Note log scale. (**b**) The quantum yield of carbon fixation ($\phi_C$, based on $^{14}$C uptake) and non photochemical quenching (NPQ) as a function of relative irradiance in the same culture. The deviation of the fit from the distribution of $\varphi_C$ at low irradiance (cf. Johnson and Barber 2003) is a consequence of forcing the fit of the PE curve through the origin. (**c**) Relationship between NPQ, measured with a Chelsea Fastracka FRR, and de-epoxidation state (DPS) in cultures of *P. provasolii* (closed symbols) and the chlorophyte *Dunaliella tertiolecta* (open symbols) incubated in darkness and at c. 60, 300 and 1000 µmol photons m$^{-2}$ s$^{-1}$ (fluorescence data from Suggett et al. 2009). Circles and triangles denote replicate cultures. (**d**) Chl*a*-specific absorption spectra for *P. provasolii* ($a^{Chl}$, heavy line) and reconstructed absorption spectra for photosynthetic pigments ($a_{PS}^{Chl}$, light solid and dotted lines). Reconstruction was based on partitioning $a^{Chl}$ using HPLC pigment data (Bidigare et al. 1990), on the assumption that the spectrum for MgDVP was the same as Chl*c*'s. Photosynthetic absorption spectra are from samples with minimal and maximal DPS (darkness, $a_{PS}[D]$, solid line; high light, $a_{PS}[Q]$, dotted line). The ratio of photosynthetic absorption with maximum DPS to photosynthetic absorption in the dark-acclimated state is also shown (dashed line)

of a saturating flash, in the dark ($F_0$, $F_m$) or in the presence of actinic illumination ($F$, $F_m'$). $F$ rises with irradiance as the quantum yield of photosynthesis, and hence the probability of energy transfer into photosynthetic pathways, declines (Fig. 11b). In contrast, the maximum fluorescence ($F_m$, $F_m'$) declines with irradiance, a change that can be expressed as non-photochemical quenching (NPQ = $[F_m - F_m']/F_m'$), as shown in Fig. 11b. The effect of varying irradiance on $Fl^{Chl}$ can be minimized by blocking electron transfer with DCMU (e.g., Gaevsky et al. 2005) or by dark-adapting the sample being interrogated. Measuring $F_m$ rather than $F_0$ has the advantage that it maximizes signal strength. In practice, any instrument that is used in flow-through mode will allow at least partial relaxation of photosynthetic induction ($F$ tends to $F_0$) or NPQ ($F_m'$ tends to $F_m$), provided that the plumbing is opaque. Instruments that interrogate natural samples *in situ* without shielding can and will be confounded by the effect, as noted shortly after fluorometry was proposed as a tool for studying phytoplankton (Kiefer, 1973a, b).

Although variability in $Fl^{Chl}$ can and does bias the estimate of Chl*a* from fluorescence (Eq. 2), the degree to which it might bias the taxonomic classification will depend on the magnitude of NPQ and its underlying cause. One mechanism that correlated with NPQ is the xanthophyll cycle (Demmig-Adams 1990), in which rapid de-epoxidation converts a photosynthetic carotenoid into a photoprotective one. In the chlorophytes, sequential de-epoxidations convert violaxanthin to antheraxanthin to zeaxanthin; and in chromophytes, a single de-epoxidation converts diadinoxanthin to diatoxanthin. As can be seen (Fig. 2b), there is a reduction in the $S_1$ energy level that results in a change in the ratio of these photoprotective to photosynthetic carotenoids. The degree of interconversion can be expressed as the de-epoxidation state, DPS (Casper-Lindley and Björkman 1998):

$$DPS = \frac{0.5[A]+[Z]}{[V]+[A]+[Z]} \tag{4}$$

or

$$DPS = \frac{0.5[DT]}{[DD]+[DT]} \tag{5}$$

in which *[V], [A], [Z], [DD]* and *[DT]* are the concentrations of, respectively, violaxanthin, antheraxanthin, zeaxanthin, diadinoxanthin and diatoxanthin. The magnitude of NPQ may be correlated with DPS, as is shown for *Pycnococcus provasolii* (Fig. 11c) or may be independent of it (Arsalane et al. 1994; Casper-Lindley and Björkman 1998; Koblizek et al. 2001), as is shown for *Dunaliella tertiolecta* (Fig. 11c) and as is seen in the cyanobacteria, rhodophytes, cryptophytes and euglenophytes, which lack a xanthophyll cycle but still generate NPQ. In one sense, the de-epoxidation is spectrally neutral, as the dissipatory step is invoked at the $S_1$ energy level of Chl*a*. This is lower than the $S_2$ or higher absorption maxima of the accessory pigments whose relative abundance defines the SFS (Fig. 2a), so photons absorbed by any pigment that contributes to the SFS should have an equal opportunity of being dissipated as heat rather than being re-emitted as fluorescence. In this sense, fluorescence quenching by the xanthophyll cycle will operate through the effective quantum yield, $\phi(\lambda_{Ex,Em})$, rather than the absorption term, $a_{PS}^{Chl}(\lambda_{Ex})$ in Eq. 1. The contribution of the xanthophylls may also act through the absorption term where there is a significant change in the xanthophyll:Chl*a* ratio, as can occur in response to short-term exposure to bright light (Olaizola and Yamamoto 1994), under acclimation over a light gradient (reviewed by MacIntyre et al. 2002), or in response to nutrient limitation (Sosik and Mitchell 1991).

However, if the epoxidated forms of the xanthophylls are significant contributors to photosynthetic absorption, then de-epoxidation could alter the SFS. This is illustrated by modeling the photosynthetic absorption spectrum by partitioning total absorption between the contributions of photosynthetic and non-photosynthetic pigments (Bidigare et al. 1990), and assuming that the effect of pigment packaging is constant at a given wavelength (cf., Geider et al. 1998). The predicted change in $a_{PS}^{Chl}(\lambda_{Ex})$ for *Pycnococcus* (Fig. 11c) is shown in Fig. 11d. The observed xanthophyll interconversion makes no difference to $a_{PS}^{Chl}(\lambda_{Ex})$ at wavelengths above 550 nm but could cause a reduction of up to 40% at lower wavelengths. In the case of SFS generated with the AOA (see previous sections), this would cause a steepening of the SFS between the 470 and 525 nm excitation bands: the modeled reduction in $a_{PS}^{Chl}(\lambda_{Ex})$ is 10% at 470 nm but 26% at 525 nm. Because *Pycnococcus* is a prasinophyte, its SFS is closest to the chlorophyte's, so this would be analogous to the steepening of *Dunaliella's* SFS under nutrient starvation (Fig. 9a). The xanthophyll cycle would make *Pycnococcus'* SFS less, not more, similar to the other eukaryotes' (Fig. 9e), and there should be no consequent

error in taxonomic classification due to xanthophyll cycle activity (cf. Fig. 10a).

Cryptophytes and cyanobacteria lack the xanthophyll cycle, but NPQ is correlated with DPS in chromophytes (Casper-Lindley and Björkman 1998; Koblizek et al. 2001). As chromophytes' SFS are typically differentiated on the basis of the presence of photosynthetic carotenoids, xanthophyll cycle activity might bias their signatures towards the chlorophytes', resulting in a bias in taxonomic classification. The degree to which this might occur is difficult to predict: it would depend on the irradiance to which the cells are acclimated (hence the quota of xanthophylls relative to other pigments, see MacIntyre et al. 2002), the intensity and duration of the irradiance to which they are exposed (Fig. 11b, c, cf. Arsalane et al. 1994; Olaizola and Yamamoto 1994), and to adaptive differences between species (Sakshaug et al. 1987; Strzepek and Harrison 2004; Lavaud et al. 2007).

In addition to the xanthophyll cycle, short-term quenching may involve state transitions. This is likely the factor that causes the large change in NPQ in the absence of significant de-epoxidation in *Dunaliella* (Fig. 11c). State transitions involve the migration of a proportion of light-harvesting complexes or phycobilisomes between PSII and PSI. The response is driven by redox control (reviewed by Kruse 2001; Allen 2002), and induction of State 2 (migration of antennae to PSI) occurs when PSII activity exceeds that of PSI at high irradiance (Schubert et al. 1995; Campbell and Oquist 1996) or in response to the demands of nitrite reduction (Sahay et al. 2006). State transitions are well documented in chlorophytes and cyanobacteria and may play a dominant role in energy dissipation in the former, even though they have a functional xanthophyll cycle (Garcia-Mendoza et al. 2002; Ross et al. 2008). State transitions also occur in cyanobacteria during light/dark transitions (Schubert et al. 1995; Campbell and Oquist 1996). They are not thought to occur in chromophytes (Owens 1986). State transitions reduce $a_{PS}^{Chl}$ at PSII, so will reduce $Fl^{Chl}$ under State 2 conditions relative to State 1. They have the potential to alter the SFS because of the unequal distribution of pigments between the antenna and the reaction center. Chlorophyll *b* and the (trace quantities of) photosynthetic carotenoids are associated with the antenna in chlorophytes (Yamamoto and Bassi 1996) and the phycobilins are associated with the phycobilisome's rods in cyanobacteria (Gantt et al. 1979; Gantt 1996). Consequently the relative abundance of accessory pigments to that of Chl*a* at PSII will decline in State 2. Because of the co-location of accessory pigments, their relative abundance at PSII should not be affected. The sensitivity of the SFS to state transitions will depend on the degree to which it is weighted by accessory pigment to Chl*a* ratios.

We performed empirical tests of the effect of inducing NPQ on both the taxonomic classification and estimates of biomass. The tests were performed on the calibration species; the chlorophyte *Dunaliella tertiolecta*, the cryptophyte *Rhodomonas lens*, the cyanobacterium *Synechococcus bacillaris,* and the diatom *Thalassiosira pseudonana*; as well as on two other chromophytes (the dinoflagellate *Amphidinium carterae*, and the prymnesiophyte *Emiliania huxleyi*). The cultures were grown at optically-thin densities under nutrient-replete conditions at c. 80 µmol photons $m^{-2}$ $s^{-1}$. Sample cultures were then dark-acclimated for 20 min to allow NPQ to relax, illuminated at 800 µmol photons $m^{-2}$ $s^{-1}$ for 40–50 min, then returned to darkness. Continuous assessments of taxonomic status and estimates of Chl*a* were made using the AOA. Pigment concentrations were determined at the beginning, midpoint and end of the light period. In all cases, there was no significant (>1%) change in the taxonomic classification, although *Amphidinium* and *Emiliania* were consistently identified as 15% chlorophytes/85% chromophytes and 60% chlorophytes/40% chromophytes, respectively. We emphasize that this result is not general: the sensitivity of the SFS to the short-term quenching mechanism will depend on both the physiological status of the organisms being investigated and on the wavelengths used to construct the SFS. Although the experimental irradiance was 10*x* the growth irradiance, the magnitude of DPS was relatively low (<0.4 in those species with a xanthophyll cycle). Had the cultures been acclimated to higher irradiance, a comparable shift in irradiance might have caused higher quenching and biased the SFS. Also, had the SFS included significant direct excitation of Chl*a*, taxonomic bias would have been more likely. Although there was no significant change in taxonomic assignment, estimates of biomass fell as fluorescence was quenched and rose as quenching was relaxed. The response of the diatom *Thalassiosira pseudonana* is shown in Fig. 12a.

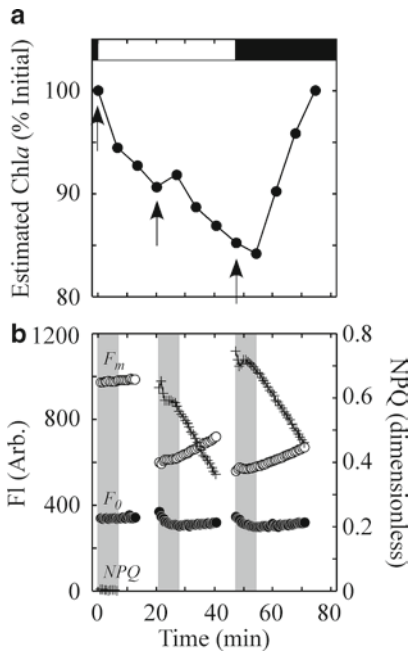


**Fig. 12** (**a**) Time-course of Chl*a* estimates on a dark-acclimated culture of the diatom *Thalassiosira pseudonana* exposed to c. 50 min of high irradiance (10*x* growth irradiance) and then returned to darkness (light and dark bars at top of panel). Estimates were made with *bbe* Moldaenke's AOA. Chl*a* is expressed relative to the $T_0$ value. Arrows indicate sub-samples removed to darkness. (**b**) Time-courses of minimum and maximum fluorescence ($F_0$ and $F_m$) and non photochemical quenching (NPQ) in subsamples from (a). Samples were held in darkness and monitored continuously with a Walz WaterPAM. Grey bars show the duration of the repeated measurements made on a single sample by the AOA (a)

A factor that affects the sensitivity to short-term quenching is the degree to which relaxation is possible before or while the measurement is being made. The data shown in Fig. 12a are averages of repeated interrogations over an interval of ca. 7 min, and made on a sample drawn into a darkened interrogation chamber rather than left under the ambient illumination. The first-order time constants for induction/relaxation of the xanthophyll cycle are relatively short, *ca*. 0.1 $min^{-1}$ in the chlorophyte *Chlorella vulgaris* (Goss et al. 2006), which would allow a significant relaxation of the fluorescence quenching during measurement. Time constants for state transitions are comparably short (Schubert et al. 1995). This is illustrated in Fig. 12b, which shows short-term changes in samples removed from the time-course experiment. The first was taken pre-illumination and shows the dark-adapted levels of $F_0$, $F_m$, and NPQ. The second, taken after 20 min of illumination shows the relaxation of quenching. The kinetics of relaxation of $F$ to $F_0$ and $F_m'$ to $F_m$ are both biphasic. The former had a rapid exponential decline ($\tau$ = 0.57 ± 0.04 $min^{-1}$), followed by a slower and approximately linear rise (0.33 ± 0.04% of $F_0$ $min^{-1}$). Relaxation of $F_m'$ was slower. There was an initial rise over 2 min that was too short to resolve by curve-fitting, followed by a linear rate (0.76 ± 0.01% of $F_m$ $min^{-1}$). Consequently, while the initial values of $F$ and $F_m'$ were 108 and 61% of $F_0$ and $F_m$, respectively, the values integrated over 7 min were 95 and 64%. Similar patterns, but with slower kinetics, were observed after 47 min of illumination (Fig. 12b). Because the magnitude of the quenching depends on both the intensity and duration of illumination (Fig. 11a, 12a), and because there are taxon-specific differences in the irradiance-dependence of both $F$ and $F_m'$ (see next section), we can not be more specific about the effect of allowing some relaxation to occur on the estimates of fluorescence. In general, though, measurements taken in darkness will have less quenching than those taken under actinic illumination and will be less likely to bias the SFS.

## 4 Optical Indices and Application of the SFS Approach in the Field

Phytoplankton are not the only colored materials in their environment. Other optically-active materials, which include water itself, chromophoric dissolved organic material (CDOM) and suspended sediments and particulate organic material (detritus), all attenuate light, so have the ability to modulate both excitation and emission. Alteration of the excitation beam affects $Fl^{Chl}$ through changes in the excitation irradiance ($E(\lambda_{Ex})$ in Eq. 1). Alteration of the emission beam affects $Fl^{Chl}$ through variation in the effective quantum yield ($\phi(\lambda_{Ex,Em})$ in Eq. 1). Because the excitation beam in a fluorometer is typically collimated, both absorption and scattering (the inherent optical properties that determine attenuation) will tend to attenuate $E(\lambda_{Ex})$. However, scattering can also augment $E(\lambda_{Ex})$ through the phenomenon of path-length amplification: the probability of a photon impinging on a particle and being absorbed is increased when photons that have not been absorbed are scattered back into the optical

path. In contrast to the excitation beam, fluorescence emission is isotropic (i.e. has an equal probability of occurring in all directions). If the photon is emitted within the cone of detection and towards the detector, it will be observed. In the case of a closed-cavity instrument, the signal can be amplified by use of reflectors that redirect fluorescence emitted in other directions towards the detector. Particles that scatter the fluorescence emission back towards the detector operate in similar fashion.

Because both absorption and scattering are spectrally-dependant, they have the potential to bias the SFS. The spectral variation for a representative estuarine water-mass is shown in Fig. 13a. While the shape of the phytoplankton absorption spectrum depends on the relative abundance of pigments with differing absorption characteristics, the shapes of the CDOM and detrital absorption curves are highly conservative (Roesler and Perry 1995), following an approximately exponential decline through the visible wavelengths:

$$a(\lambda) = a(400)e^{-\sigma(\lambda-400)} \quad (6)$$

where $a(\lambda)$ and $a(400)$ are absorption at λ and 400 nm ($m^{-1}$); and $\sigma$ is the spectral slope ($nm^{-1}$). Absorption by phytoplankton, CDOM and detritus depends on their relative concentrations: absorption by water is constant, as is its scattering. The latter is very small, less than 0.006 $m^{-1}$ between 400 and 700 nm (Buiteveld et al. 1994), which is less than 0.2% of the total scattering shown in Fig. 13a, and makes no significant contribution in most estuarine and coastal waters. The spectral dependence of scattering has the potential to be more variable than the dependencies of the components of

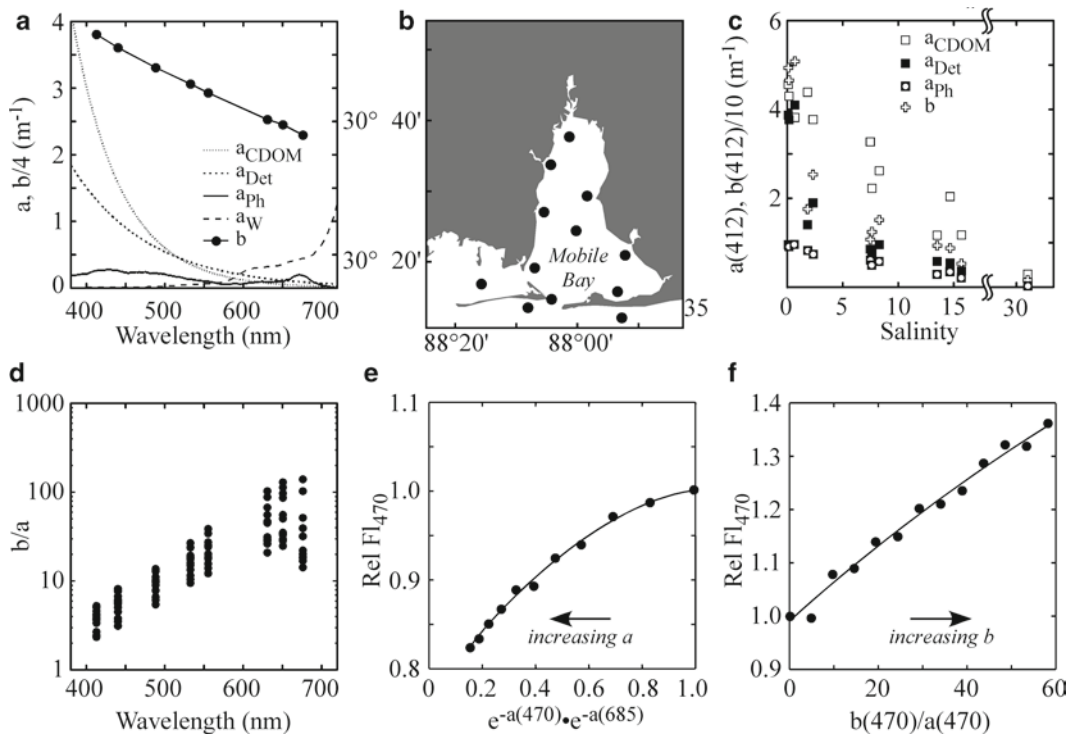


**Fig. 13** (**a**) Absorption (*a*) and scattering (*b*) spectra for a representative sample from Mobile Bay, USA. Note different scales for *a* and *b*. Absorption by CDOM ($a_{CDOM}$), detritus ($a_{Det}$) and phytoplankton ($a_{Ph}$) were measured on material retained on ($a_{Det}$ and $a_{Ph}$) and passing ($a_{CDOM}$) a GF/F filter. Absorption enhancement on the filter was corrected using coefficients from Lohrenz (2000). Absorption by water ($a_W$) is from Pope and Fry (1997) and van Kee (cited by Mueller 2003). Scattering coefficients were estimated using an ac-9 (WETLabs, Philomath, OR), corrected according to Gallegos and Neale (2002). (**b**) Map of Mobile Bay, USA, showing locations of sample sites. Latitude and longitude are °N and °W. (**c**) Variation of absorption and scattering at 412 nm (*a*(*412*) and *b*(*412*)) as a function of salinity at the sample sites. Note different scales for *a* and *b*. (**d**) Variation in the ratio of scattering to total absorption (*b*/*a*) with wavelength at the sample sites. Note log scale. (**e**) Variation in relative fluorescence of Basic Blue 3 excited at 470 nm with increasing concentrations of CDOM, as a function of the absorption parameter (see text for details). The line is a 2nd-order polynomial fit. (**f**) Variation in relative fluorescence of Basic Blue 3 excited at 470 nm with increasing concentrations of Maalox as a function of *b*/*a* (see text for details). The line is a 2nd-order polynomial fit

absorption, as the efficiency of scattering depends on the ratio of particle diameter to wavelength (van de Hulst 1957). The scattering coefficient may therefore increase, decrease or be approximately constant through the visible wavelengths, depending on the size of the particles (Morel 1991; Ahn et al. 1992).

The relative contributions of the materials other than water to absorption and scattering vary with water type. Absorption is dominated by CDOM and detritus in most coastal and estuarine (Case II) waters and dominated by water and phytoplankton in most pelagic (Case I) waters. In the former, there is usually a strong variation with salinity, reflecting terrestrial inputs, as is illustrated with data collected on a single day in Mobile Bay, a semi-tropical estuary on the northern Gulf of Mexico (Fig. 13b, c). Note that absorption at 412 nm by phytoplankton is relatively minor compared to absorption by CDOM and detritus (11–18% of the sum of $a_{CDOM}$ and $a_{Det}$). The high load of suspended sediments is also manifested in the ratio of scattering to total absorption (the sum of $a_{CDOM}$, $a_{Det}$, $a_{Ph}$ and $a_W$), *b/a* (Fig. 13d). Because the magnitudes of absorption and scattering are not constant, between sites or between wavelengths, they have the potential to bias the SFS in two ways. The first is through direct optical interference in the spectral fluorescence measurements that are compared with the calibration SFS for taxonomic classification. The second is indirect and is related to differences in light absorption and quenching between representatives of different taxa. The spectral characteristics of the underwater light regime are driven by variability in the ratio of chromophores that absorb strongly at short wavelengths (CDOM, detritus and phytoplankton) vs water, which absorbs strongly at long wavelengths. Consequently, the light absorbed by different taxa, which reflects their pigment complement and determines $F^{Chl}$, will not be the same, either between taxa or between water bodies. We model the magnitude of these in turn, using data collected in Mobile Bay (Fig. 13).

## 4.1 Bias in SFS by Background Absorption and Scattering

We can investigate the potential interference of background absorption and scattering by modeling optical interference under the conditions at each site, using the SFS generated with the AOA (Fig. 5a). Although the effects of absorption and scattering are interactive, we can treat them independently as a first approximation. The effect of variable absorption in the absence of changes in scattering was tested by measuring fluorescence from solutions of the fluorescing aniline dye Basic Blue 3 (Kopf and Heinze 1984) with additions of purified CDOM (Suwannee River humic acid, International Humic Substances Society). The additions corresponded to the range observed at the Mobile Bay stations, 0–6 $m^{-1}$ at 400 nm (0–4.91 $m^{-1}$ at 412 nm, cf. Fig. 13c). From first principles, we would expect the signal to be attenuated for both the excitation and emission in proportion with an absorption parameter defined as $exp(-a(\lambda_{Ex}))\bullet exp(-a(\lambda_{Em}))$. A full description of the attenuation would require definition of the effective optical path-length(s). In practice these are very difficult to define as the signal is the integral of multiple effective path-lengths and weighted by the response of fluorophores that are closest to the detector (Serôdio 2004). The relationship between fluorescence, expressed relative to fluorescence in the absence of a CDOM addition, and the absorption parameter is shown in Fig. 13e, calculated for 470 nm excitation and 685 emission. Note that the value of the parameter falls as absorption by CDOM increases. The relationship could be fit well with a second-order polynomial ($R^2$ = 0.995). The effect of scattering in the absence of absorption was tested using dilutions of Maalox, a suspension of aluminum hydroxide and magnesium hydroxide particles. The dilutions were made to match the range of scattering observed at 412 nm in the Mobile Bay samples (0–36 $m^{-1}$, *b/a* 0 – 58.2; Fig. 13c, d). As anticipated, the path-length enhancement caused relative fluorescence to rise. A second-order polynomial provided a marginally better fit than a first-order (linear) equation (RMS = 0.014 vs 0.015; $R^2$ = 0.993 vs 0.991, Fig. 13f).

The effect of optical interference by background absorption and scattering on the SFS was then modeled by calculating the cumulative effects of absorption (Fig. 13e) and scattering (Fig. 13f) for each excitation wavelength, parameterized with the spectral data collected at each site (Fig. 13a, c and d). The effect of total non-water absorption (the sum of $a_{CDOM}$, $a_{Det}$ and $a_{Ph}$) was assumed to follow the same relationship as was observed for the Suwannee River CDOM in the test. The contributions of water were not included as the

instrument was calibrated on aqueous suspensions. The effect of scattering was assumed to follow the same relationship as the Maalox, although the particles present in the natural samples will likely include a wider size-range. As both the efficiency and angular distribution of scattering vary with size, the Maalox is likely to be an imperfect substitute for the natural assemblage of particles. If the latter have a mean volume scattering function that is more or less isotropic (i.e., with an angular distribution that is weighted less or more towards the forward angle) than the Maalox, the relationship in Fig. 13f will tend to under- or over-estimate the enhancement of fluorescence, respectively.

Because the contributions of CDOM and detritus to absorption decline more rapidly with wavelength than does scattering (Fig. 13a), the relative reduction in fluorescence due to absorption declines with wavelength more rapidly than does the enhancement due to scattering. In short, the bias is more negative at short than long wavelengths. When the calibration SFS (Fig. 5a) were weighted for the reduction by absorption and enhancement by scattering at each wavelength and re-normalized, the spectral bias was manifested as an anti-clockwise rotation in the Norm SFS between the 470 and 535 nm channels in the eukaryotes and between 525 and 570 nm in the cyanobacterium (Fig. 14a–d). The biased SFS that would be detected from the chlorophyte (*Dunaliella*) have a higher similarity to the cyanobacterium (*Synechococcus*) because the chlorophyte's SFS has the steepest decline between 470 and 570 nm and the steepest rise between 570 and 610 nm (Fig. 5a). This can be seen in the ordination of the similarity matrix (Fig. 14e), and would result in a degree of mis-identification as a mixture of chlorophytes and cyanobacteria. The bias in signal from the chromophyte (*Thalassiosira*) makes it more similar to the cryptophyte (*Rhodomonas*), which has the flattest SFS of the eukaryotes between 470 and 570 (Fig. 5a). In consequence, the biased signals would result in a degree of mis-identification as a mixture of chromophytes and cryptophytes. Because the cryptophyte has the flattest decline between 470 and 570 nm of the three eukaryotes, a further flattening makes it less, not more, like the other eukaryotes. Because its SFS declines between 570 and 610 nm, the rotational bias will make it slightly more like the cyanobacterium (Fig. 14e). The biased signals would result in a degree of mis-identification as a mixture of cryptophytes and cyanobacteria. Only the cyanobacterium would be immune from mis-classification. As it has the SFS with the steepest rise between 570 and 610, the steepening of the rise caused by the rotational bias makes the signal less, not more, like the

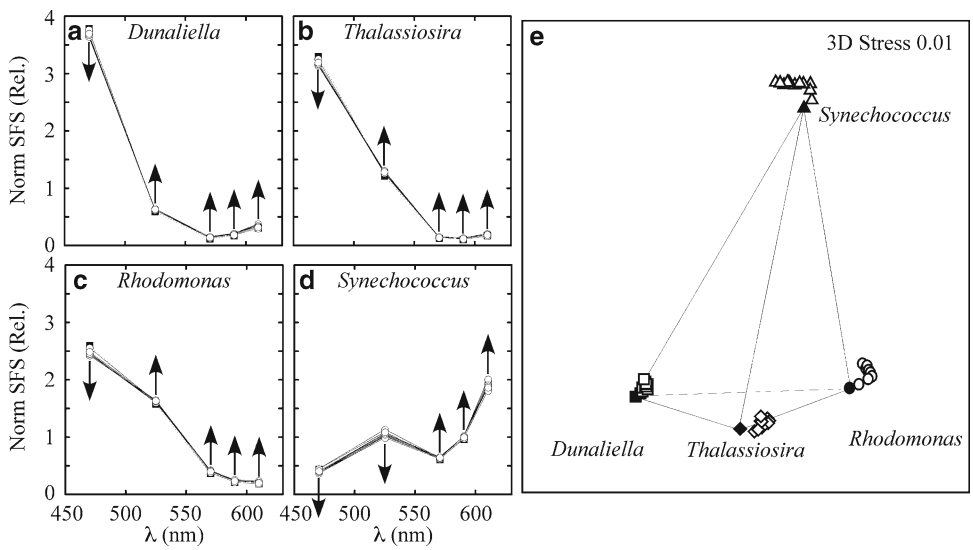


**Fig. 14** Changes in the Norm SFS for (**a**) the chlorophyte *Dunaliella tertiolecta,* (**b**) the chromophyte (diatom) *Thalassiosira pseudonana,* (**c**) the cryptophyte *Rhodomonas lens* and (**d**) the cyanobacterium *Synechococcus bacillaris* modeled with varying degrees of optical interference (see text for details). Arrows denote the net direction of change relative to the calibration values at each wavelength. (**e**) Multidimensional scaling plot of the Norm SFS from **a–d** (open symbols) superimposed on the calibration signatures (closed symbols, cf. Fig. 5c)

eukaryotes (Fig. 14e) and the biased signals should cause no change in the taxonomic classification.

## 4.2 Quenching In Situ and Taxonomic Assessment

The spectral dependence of light penetration through a water column is a function of the relative abundance of the optically-active materials in it. Because representatives of the different taxa differ in the distribution of photosynthetic pigments, the light-absorption by each ($a_{PS}^{Chl}(\lambda_{Ex})$) would differ, depending on whether attenuation were weighted towards long wavelengths (domination by water; Case I waters) or towards the short wavelengths (domination by CDOM and detritus; Case II). Because fluorescence is in turn determined by the rate of light absorption (Fig. 11a), this could be manifested as differences in apparent abundance of each group. We consider this by modeling light attenuation and absorption for the four calibration species used so far. Their specific absorption spectra are shown in Fig. 15a, as is a mean curve for a population containing equal biomass (as Chl*a*) of each. This mean spectrum was used with measurements from the clearest and most turbid samples in Fig. 13 to model downwelling irradiance profiles (Fig. 15b, c). Briefly, incident noon-time spectral irradiance was modeled according Greg and Carder (1990). The model was parameterized with records of air temperature, wind speed, atmospheric pressure and relative humidity from the center of Mobile Bay (http://www.mymobilebay.com/) and with UV and visibility data that were obtained from NOAA's National Weather Service. Spectral attenuation of the incident irradiance was modeled from sun angle (determined from latitude and date/time), and the spectral dependencies of total absorption and scattering (Kirk 1994), as described in more detail by MacIntyre et al. (2004). Total absorption was defined as the sum of $a_{CDOM}$, $a_{Det}$, and $a_{Ph}$, measured for the field samples, and $a_W$ (cf. Fig. 13a). Variation in absorption was driven by differences in the magnitude rather than shape of the spectra: $a_{CDOM}(400)$ and $a_{Det}(400)$ varied by 12*x* and 60*x* (max/min), respectively, while the spectral slopes, σ (Eq. 6), differed by only 1.2*x* and 1.3*x*. Absorption by phytoplankton, $a_{Ph}(\lambda)$, was defined by the product of the mean Chl*a*-specific absorption spectrum (Fig. 15a) and Chl*a* concentration measured at the site. Absorption by water was given by Pope and Fry (1997). For comparison, at the clearest site (Fig. 15b) $a_{CDOM}(400)$ = 0.41 $m^{-1}$; $a_{Det}(400)$ = 0.16 $m^{-1}$; Chl*a* = 1.99 mg $m^{-3}$; at the most turbid site (Fig. 15c) $a_{CDOM}(400)$ = 3.66 $m^{-1}$; $a_{Det}(400)$ = 9.72 $m^{-1}$; Chl*a* = 1.05 mg $m^{-3}$. The water columns were assumed to be vertically homogenous.

The spectral dependency of irradiance is shown at 0, 1, 2, 3, 4 and 5 optical depths (surface and the depths at which irradiance in the visible, 400–700 nm, is attenuated by five successive *e*-foldings, to 36.8, 13.5, 4.98, 1.83 and 0.67% of surface irradiance) in Fig. 15b and c. Note the spectral shift between the subsurface dominance of irradiance at c. 550 nm (green light) at the clear site and the dominance of irradiance at c. 660 nm (red light) at the turbid site. At any depth, the light absorbed by each of the four taxa that constitutes the assemblage can be calculated as:

$$E_{abs} = \sum_{\lambda=400}^{\lambda=700} E_z(\lambda) a^{Chl}(\lambda) \quad (7)$$

where $E_{abs}$ is Chl*a*-specific light absorption (μmol photons [mg Chl*a*]$^{-1}$ $s^{-1}$); $E_z(\lambda)$ is spectral irradiance at depth *z* and wavelength $\lambda$ (μmol photons $m^{-2}$ $s^{-1}$ $nm^{-1}$); and $a^{Chl}(\lambda)$ is Chl*a*-specific light absorption at wavelength $\lambda$ ($m^2$ [mg Chl*a*]$^{-1}$). However, this description includes absorption by non-photosynthetic pigments, which over-estimates the light that can be re-emitted as fluorescence.

Light absorption by photosynthetic pigments was modeled by decomposing $a^{Chl}(\lambda)$ into the contributions of photosynthetic and non-photosynthetic pigments using published estimates of *in vivo* absorption by different pigment classes (Bidigare et al. 1990) and the spectral dependence of the pigment packaging coefficient (Geider et al. 1998), illustrated in Fig. 11d. The approach is an approximation because of variation in the packaging coefficient that is not accounted for in the spectral reconstruction (Johnsen et al. 1997; Bricaud et al. 2004). Absorption by PC in the cyanobacterium (*Synechococcus*) was estimated from the absorption of Phycocyanin 645 in acidic urea (MacColl and Guard-Friar 1983). The photosynthetic absorption spectra, $a_{PS}^{Chl}(\lambda)$, are shown in Fig. 15d. Note the peak at c. 550 nm due to PE in the cryptophyte (*Rhodomonas*) and the peak at c. 645 due to PC in *Synechococcus*. Note also the difference between the chlorophyte (*Dunaliella*) and diatom (*Thalassiosira*) at c. 450–550 nm

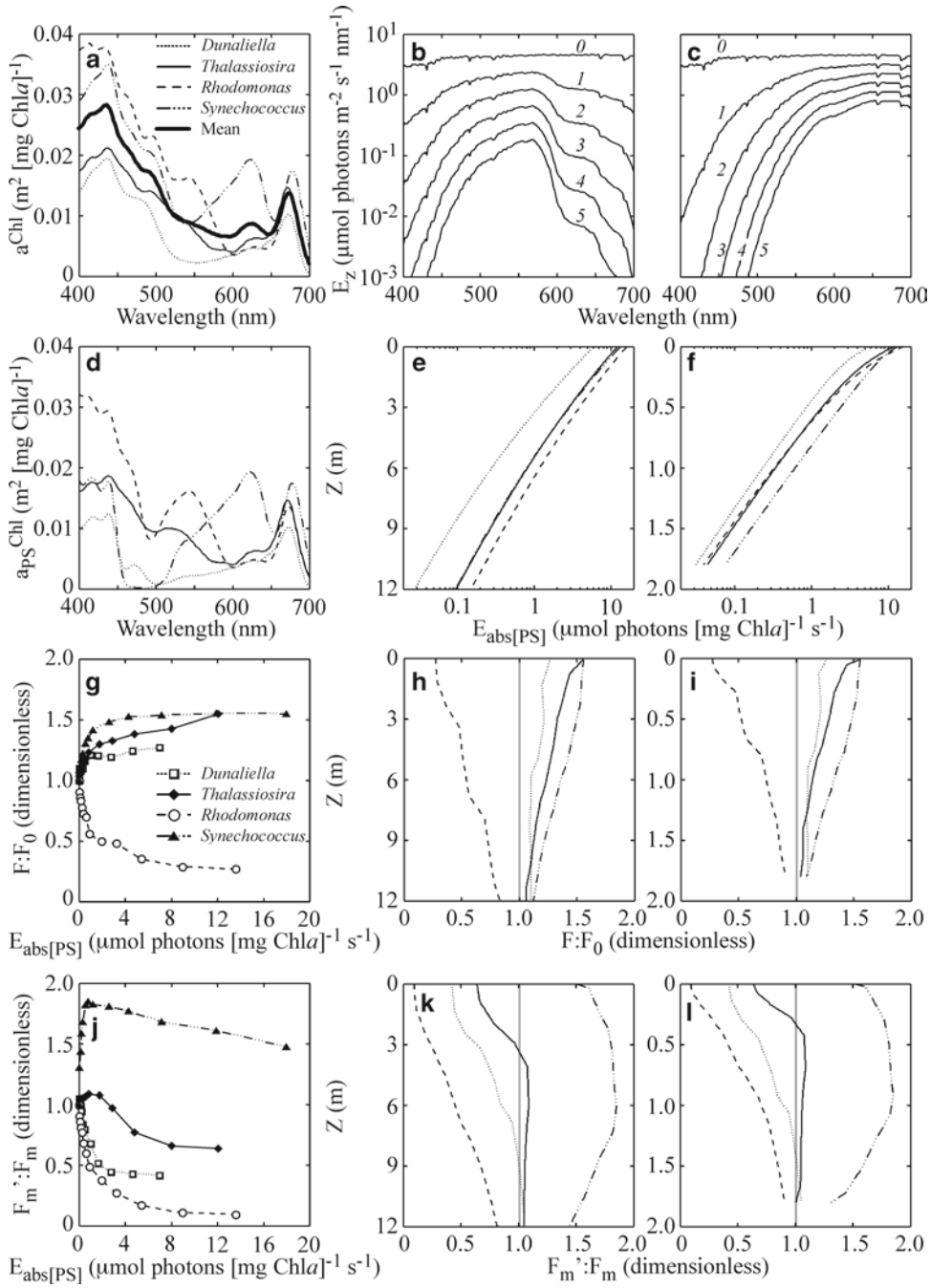


**Fig. 15** Effect of submarine irradiance on fluorescence, modeled for the least (**b, e, h** and **k**) and most (**c, f, i** and **l**) turbid samples from Mobile Bay (Fig. 13) See text for details. (**a**) Chl*a*-specific absorption spectra for the chlorophyte *Dunaliella tertiolecta,* the chromophyte (diatom) *Thalassiosira pseudonana,* the cryptophyte *Rhodomonas lens* and the cyanobacterium *Synechococcus bacillaris* (light lines). The heavy line is the mean spectrum for an equal-Chl*a* mixture. The same line patterns are used in **d–l**. (**b, c**) Spectral dependence of irradiance at the surface (0) and 1, 2, 3, 4 and 5 optical depths. (**d**) Modeled Chl*a*-specific photosynthetic absorption spectra for *Dunaliella, Thalassiosira, Rhodomonas* and *Synechococcus*. (**e, f**) Depth-dependence of photosynthetically-useable light, $E_{abs[PS]}$ absorbed by the four taxa. (**g**) Variation in minimum fluorescence, expressed as a ratio to the dark-adapted state ($F:F_0$), as a function of irradiance in the four taxa. Irradiance is expressed as photosynthetically-useable light, $E_{abs[PS]}$. (**h, i**) Depth-dependence of modeled minimum fluoresence, expressed as $F:F_0$ for the four taxa. Vertical grey lines show the true (i.e. dark-adapted) value. (**j**) Variation in maximum fluorescence, expressed as a ratio to the dark-adapted state ($F_m':F_m$), as a function of irradiance in the four taxa. Irradiance is expressed as photosynthetically-useable light, $E_{abs[PS]}$. Symbols are as in (**g**). (**k, l**) Depth-dependence of modeled maximum fluoresence, expressed as $F_m':F_m$ for the four taxa. Vertical grey lines show the true (i.e. dark-adapted) value

due to the respective absence and presence of photosynthetic carotenoids. Substitution of the absorption by photosynthetic pigments, $a_{PS}^{Chl}$, for $a^{Chl}$ in Eq. 7 allows the depth-distribution of photosynthetic light absorption ($\sum[E(\lambda)\bullet a_{PS}^{Chl}(\lambda)]$ in Eq. 1) to be calculated for each taxon. These are shown in Fig. 15e and f. Light absorption at the clear site, where the subsurface irradiance peaks at wavelengths absorbed efficiently by PE, is highest for the cryptophyte (Fig. 15e). Light absorption at the turbid site, where the subsurface irradiance peaks at wavelengths absorbed efficiently by PC, is highest for the cyanobacterium (Fig. 15f). Absorption is lowest for the chlorophyte at both sites.

We modeled the fluorescence that would be emitted by each taxon under two conditions, where the excitation intensity is low enough not to cause an actinic effect and where it is high enough to saturate fluorescence ($F$ and $F_m'$, respectively). The water column was assumed to be well-mixed and the kinetics of mixing were assumed to be such that the rate of change of irradiance would permit photosynthetic induction, state transitions and xanthophyll cycling but not acclimative pigment regulation (cf. MacIntyre et al. 2000; Raateoja et al. 2009). Critically, we assume that there is a perfect correction for the confounding effects of background attenuation and scattering (see previous section). In both cases, there is no dark-acclimation, so the signal reflects the variability in $F^{Chl}$ in response to ambient irradiance, a reflection of the relative activities of photosynthetic and photoprotective mechanisms (cf. Fig. 11a, b). For the first case (no actinic effect, $F$), the fluorescence can be estimated in dimensionless terms as the ratio to $F_0$. The variation in $F{:}F_0$ for the four taxa is shown in Fig. 15g, expressed as a function of irradiance absorbed by photosynthetic pigments ($E_{abs}$, Eq. 7). Note the difference between the response of *Rhodomonas* and the other taxa. The vertical variation in fluorescence for each species is modeled for the clear and turbid water columns (Fig. 15h and i) from the depth-distributions of $E_{abs}$ and the relationships between $F{:}F_0$ and $E_{abs}$. The signals are shown in relation to the fully-relaxed condition used for calibration ($F{:}F_0 = 1$). Differences between the water-masses, driven by differences in the light regimes, are minor compared to differences between the taxa. The quenching of $F$ at all irradiances for *Rhodomonas* is the most obvious feature but the differences between the other three taxa are site-dependent. The difference between *Dunalliela* and *Thalassiosira* are more pronounced at the clear site (Fig. 15h) than at the turbid site (Fig. 15i) because the spectral shift towards long wavelengths obviates the differences in light absorption by photosynthetic carotenoids. The differences between *Synechococcus* and *Dunalliela* or *Thalassiosira* are more pronounced at the turbid site because of its enhanced relative absorption by PC (Fig. 15f vs e).

The same exercise was performed with the signals that would be excited with a saturating flash. Variation in $F_m'{:}F_m$ for the four taxa is shown in Fig. 15j and the vertical profiles, calculated as for $F{:}F_0$, are shown for the clear and turbid sites in Fig. 15k and l. The dispersion of responses among the three eukaryotes is greater at the clear site than at the turbid one because of the wider dispersion in light absorption (Fig. 15e *vs* f). The increased difference between *Synechococcus* and the eukaryotes is due to the much higher range in $F_m'{:}F_m$ in the former (Fig. 15j), which reflects in part the state transition that cyanobacteria undergo in darkness (Campbell and Oquist 1996).

The effect of the quenching on taxonomic assessment is shown in Fig. 16. The contribution of each taxon is calculated from the ratio of its fluorescence to total fluorescence. When modeled as above for equal contributions of the four taxa, there is a progressive error due to taxonomic differences in the magnitude of quenching. The error is greatest at high irradiance (i.e. near the surface). Although each taxon contributed 25% of biomass (Chl*a*), the estimated percentages of chlorophytes: chromophytes: cryptophytes: cyanobacteria were 27:33:6:33% when estimated from $F{:}F_0$ and 16:24:3:57% when estimated from $F_m'{:}F_m$ (Fig. 16a, b). The estimates were more accurate with decreasing irradiance, reaching 27:26:20:27 when estimated from $F{:}F_0$ and 24:24:19:33% when estimated from $F_m'{:}F_m$ at 5 optical depths. The estimate of Chl*a* ranged from 116% to 103% when measured from $F{:}F_0$ and from 109 to 67% when estimated from $F_m'{:}F_m$ (Fig. 16c). Distributions modeled for the turbid water site varied by less than a percentage point from these ratios in almost all cases.

The bias in taxonomic weighting and estimates of biomass depends on how representative the fluorescence-irradiance relationships are and on what combination of taxa are used in the model. The quenching observed for *Rhodomonas lens* (Fig. 15g, j), although very different from the responses of the other taxa, is not unique: we have observed similar patterns in the cryptophytes *Storeatula major* and *Proteonomas sulcata*.

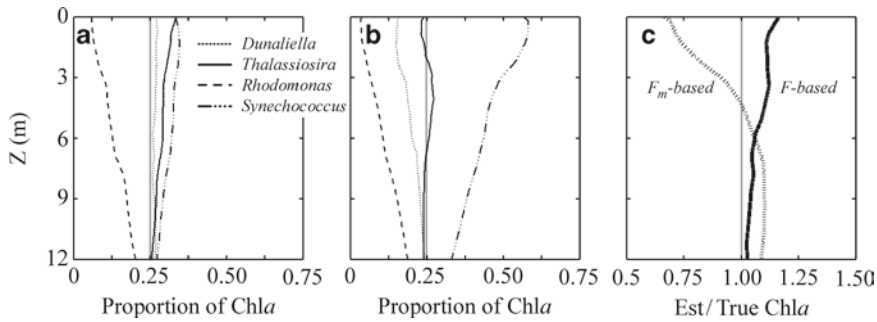


**Fig. 16** Modeled error in taxonomic assignment for an equal mixture of the chlorophyte *Dunaliella tertiolecta,* the chromophyte (diatom) *Thalassiosira pseudonana,* the cryptophyte *Rhodomonas lens* and the cyanobacterium *Synechococcus bacillaris*. (See text for details.) (**a, b**) Depth-dependence in the estimated proportion of total Chl*a* assigned to each taxonomic group. The true proportions (vertical grey lines) are all 0.25. Data are based on minimum (**a**) and maximum (**b**) fluorescence. (**c**) Depth-dependence of the error in total Chl*a*, estimated from minimum ($F$) and maximum ($F_m$) fluorescence. Chl*a* is expressed as relative to the true value (vertical grey line)

The biases shown in Fig. 16 would be weighted differently, and the bias less severe, if the model were run for a binary mixture of *Thalassiosira* and *Dunaliella*, because of the overall similarity of their fluorescence responses (Fig. 15g, j). The biases would be more severe if the model were run for a binary mixture of *Rhodomonas* and *Synechococcus* because they have the most pronounced differences in quenching responses (Fig. 15g, j).

The significance of these modeling exercises is that:

1. Errors of misidentification can be introduced into taxonomic partitioning if the algorithms are not corrected for biases introduced by other optically-active compounds;
2. Taxon-specific patterns of quenching can confound the taxonomic partitioning, causing in this case a severe underestimate of the contribution of cryptophytes; and
3. The biases in taxonomic classification depend on flash intensity.

Although using a saturating flash has the advantage of increasing the signal:noise ratio, increasing the sensitivity of the method, the errors in taxonomic assignment are more pronounced for the responses measured here. A simple solution is to make measurements at night, when quenching is relaxed (Chekalyuk et al. 2000), or to use a darkened, flow-through system that permits some relaxation of NPQ before the measurement is made (cf. Fig. 12b). While this is easily accommodated for mapping along a cruise-track or on a mooring, it is more difficult for depth-profiling instruments, where the residence time of cells in the interrogation volume can be short enough to bias measurements of the fluorescence ratio $F_q/F_v$ (Schimanski et al. 2006). In the absence of an interrogation that allows $F$ and $F_m'$ to relax towards $F_0$ and $F_m$, apparent depth-dependent variations in taxonomic composition and biomass should be treated with caution (Fig. 16). Under the modeled conditions, inter-specific variation in $F^{Chl}$ with irradiance had more of an effect on the taxonomic assessment than did differences in the spectral dependence of irradiance. Note that the model assumed a perfect correction for the biases that would be due to background absorption and scattering, which would otherwise further bias the predicted output.

## 5 A Field Test of the SFS Approach

The SFS approach has been field-tested in several locales and found to give qualitatively similar results to taxonomic classification based on microscopy or HPLC analysis of pigments (Cowles et al. 1993; Poryvkina et al. 1994; Seppälä and Balode 1998; Gaevsky et al. 2005; Gregor et al. 2005; Jakob et al. 2005; Parésys et al. 2005; Richardson et al. 2010). Robust relationships require both constrained variability in $F^{Chl}$, hence covariance between fluorescence intensity and Chl*a*, and consistent SFS. However, the past 30 years of research have shown that there is variability in $F^{Chl}$ associated with cell size, taxonomic

affiliation and physiological status (re-iterated in Fig. 6c, 7, 10–12) and we have demonstrated that physiologically-driven variability in SFS can confound taxonomic assessment (Fig. 9–10). Further interference can arise from optical interference and irradiance-driven variability in quenching (Fig. 13–16). On the face of it, the observations of qualitative similarities between fluorescence-based and microscopic- or pigment-based taxonomy and variability in $F^{Chl}$ and SFS seem difficult to reconcile.

We suggest that there are three factors that underlie the paradox. The first is that variability in $F^{Chl}$ in natural systems may be lower than the extremes observed in some lab studies. Our observations of $F^{Chl}$ suggest variation of c. 5*x* between species (Fig. 6c) and c. 2–4*x* within species subjected to simultaneous light- and nutrient-stress (Fig. 9). However, there may be less variation in the same species over wide ranges of light- or nutrient-availability when in balanced growth. While the range in $F^{Chl}$ under both nutrient-starved and nutrient-limited growth was similar, c. 2*x*, in the diatom *Thalassiosira pseudonana* (Fig. 7, 9), variability in the chlorophyte *Dunaliella tertiolecta* was 3.7*x* under nutrient starvation but only 1.7*x* under a 9*x* range of nutrient-limitated growth rates (Sosik and Mitchell 1991). We would expect to see the wide ranges characteristic of nutrient starvation under the boom-and-bust dynamics typical of blooms but these are the conditions under which top-down control is reduced. Otherwise, the reduction in growth rate associated with nutrient starvation will result in a loss of biomass, given that biomass accumulation or loss depends on the balance between productivity and grazing. Rapid removal of slowly-dividing, stressed cells by grazing will tend to dampen variation in $F^{Chl}$, as stressed cells are rapidly removed when the grazing rate exceeds the growth rate.

A second consideration is the synergistic effects of taxonomic affiliation and biomass. In many water-masses, the phytoplankton are dominated by cyanobacteria and/or pico-eukaryotes under low-biomass (oligotrophic) conditions and by eukaryotic nano- or micro-plankton under high-biomass (meso- or eutrophic) conditions (e.g. Bouman et al. 2005; Ras et al. 2008; Uitz et al. 2008). This will enhance the slope of the fluorescence-chlorophyll relationship in bulk measurements of Chl*a* fluorescence excited via chlorophylls or photosynthetic carotenoids but dampen it in bulk measurements of fluorescence excited via phycobilins. An allied point is the importance of dynamic range. Even if $F^{Chl}$ varies by 2–5*x*, then fluorescence and Chl*a* will almost certainly covary if the variability in Chl*a* approaches an order of magnitude, as can occur down salinity gradients within an estuary or with depth in a stratified water-column.

The third consideration concerns covariance of interfering chromophores. Although the potential for optical inference is highest in estuaries where both CDOM and suspended material reach high levels, the effects of absorption and scattering on signal detection may be largely compensatory. This is illustrated in Fig. 17a and b, which show variation in $a_{CDOM}(400)$ and $a_{Det}(400)$ down the salinity gradient in Mobile Bay. Samples were collected at the sites shown in Fig. 13b at approximately monthly intervals over a year. Although there are multiple sources of CDOM from the different tributaries, there is a significant correlation between CDOM absorption and salinity in each month. Regression slopes for untransformed data vary by 5.6*x* between months but the overall correlation ($R = -0.76$) is still statistically-significant ($p < 0.01$). Similarly, although detrital absorption can be driven by benthic resuspension (which is largely independent of the salinity structure), there are statistically-significant relationships between $a_{Det}(400)$ and salinity in each month and a significant overall correlation ($R = -0.63$, $p < 0.01$). Because the suspended particulate material both scatters and absorbs light, there is a significant relationship between detrital absorption and scattering (not shown). Because both CDOM and detrital absorption covary, there are also significant relationships between total absorption and scattering (Fig. 17c). The overall correlation is 0.89 ($p < 0.01$). Their effects are therefore compensatory (cf Fig. 13e, f), reducing the potential bias on detection of fluorescence signals. Although the assemblage in Mobile Bay was variously dominated by diatoms, chlorophytes, cryptophytes and cyanobacteria in different months, the regression slopes between *F* and Chl*a* (i.e. $F^{Chl}$) only varied by 2.5*x* between months and fluorescence was significantly correlated with Chl*a* concentration (Fig. 17d; overall $R = 0.86$, $p < 0.01$). This was likely because of the compensatory effects of absorption and scattering and the high dynamic range (Chl*a* concentrations varied 11*x* to 41*x* by month): changes in fluorescence are due primarily to changes in Chl*a* and secondarily to changes in $Fl^{Chl}$. We would not expect to see similar agreement in locales where the optical interference by absorption is not compensated

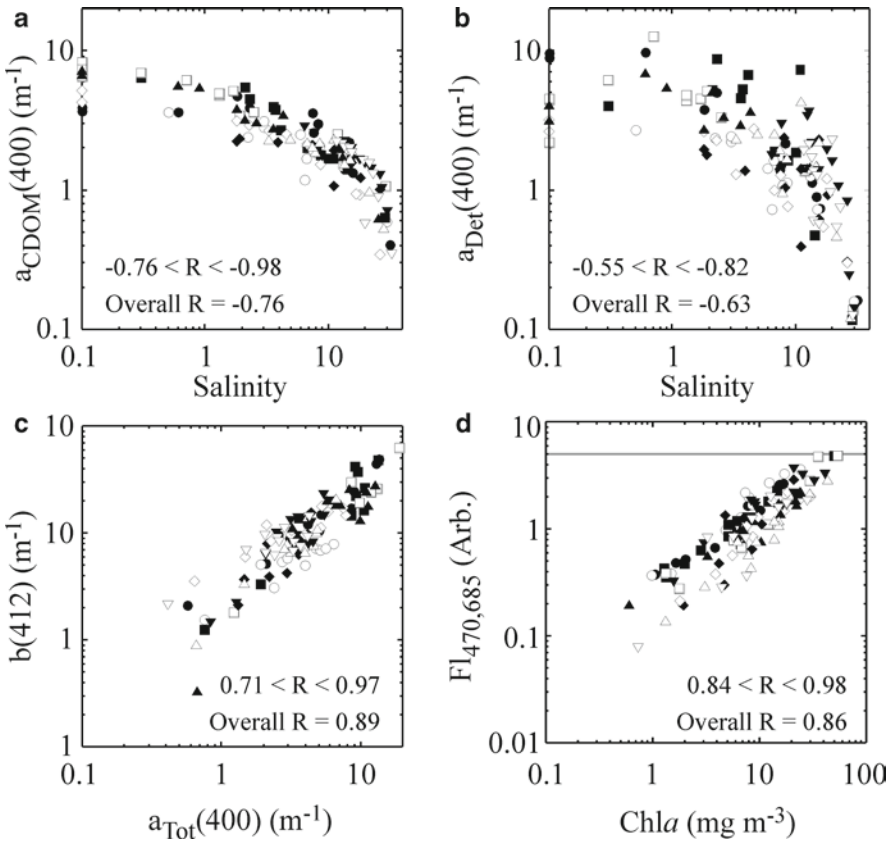


**Fig. 17** Variation in optical parameters and Chl*a* in Mobile Bay. Sites (Fig. 13B) were sampled approximately monthly between December, 2004, and October, 2005. Different symbols are for each sample trip. Correlation coefficients are shown for each trip and for the combined dataset (*Overall*). All correlations were statistically significant ($p < 0.01$). (**a**) Variation in absorption by CDOM with salinity. Regression slopes varied by 5.6*x* between trips. (**b**) Variation in absorption by detritus with salinity. Regression slopes varied by 3.9*x* between trips. (**c**) Variation in scattering with total absorption (the sum of $a_{CDOM}(400)$, $a_{Det}(400)$, $a_{Ph}(400)$ and $a_{W}(400)$). Regression slopes varied by 3.8*x* between trips. (**d**) Variation in fluorescence with Chl*a* concentration. Fluorescence was measured with a SeaPoint Sensors Chl*a* Fluorometer. The grey line indicates sensor saturation. Regression slopes varied by 2.5*x* between trips

for by scattering (e.g. in chromophoric lakes with low seston concentrations), nor where the dynamic range in Chl*a* was small.

Given that there were robust relationships between fluorescence and phytoplankton abundance at the study site, we conducted a field test of the AOA's ability to discriminate between taxa on a transect from Mobile Bay into the Gulf of Mexico. Discrete samples were taken at 11 stations (Fig. 18a) to ground-truth the AOA. Pigment concentrations of material retained on Whatmann GF/F filters were measured by HPLC (Van Heukelem and Thomas 2001) and CDOM absorption was measured on the filtrate. The water was sampled at c. 0.5 m below the surface with a diaphragm pump and flowed through a YSI CT sonde and the AOA. Variations in salinity and temperature are shown in Fig. 18b. The AOA was used with the calibrations derived from laboratory testing (see above), based on nutrient-replete cultures of a representative chlorophyte (*Dunaliella tertiolecta*), chromophyte (the diatom *Thalassiosira pseudonana*), cryptophyte (*Rhodomonas lens*) and the PC-rich cyanobacterium (*Synechoccus bacillaris*). The AOA estimates CDOM concentration from CDOM fluorescence, excited with a UV LED, and uses the data to correct the classification of phytoplankton type and abundance. A further correction is based on transparency in the interrogation cavity, which provides a first-order correction for absorption and scattering (cf. Fig. 13). The AOA's estimates of Chl*a* and CDOM are shown in Fig. 18c. Both rose with proximity to the

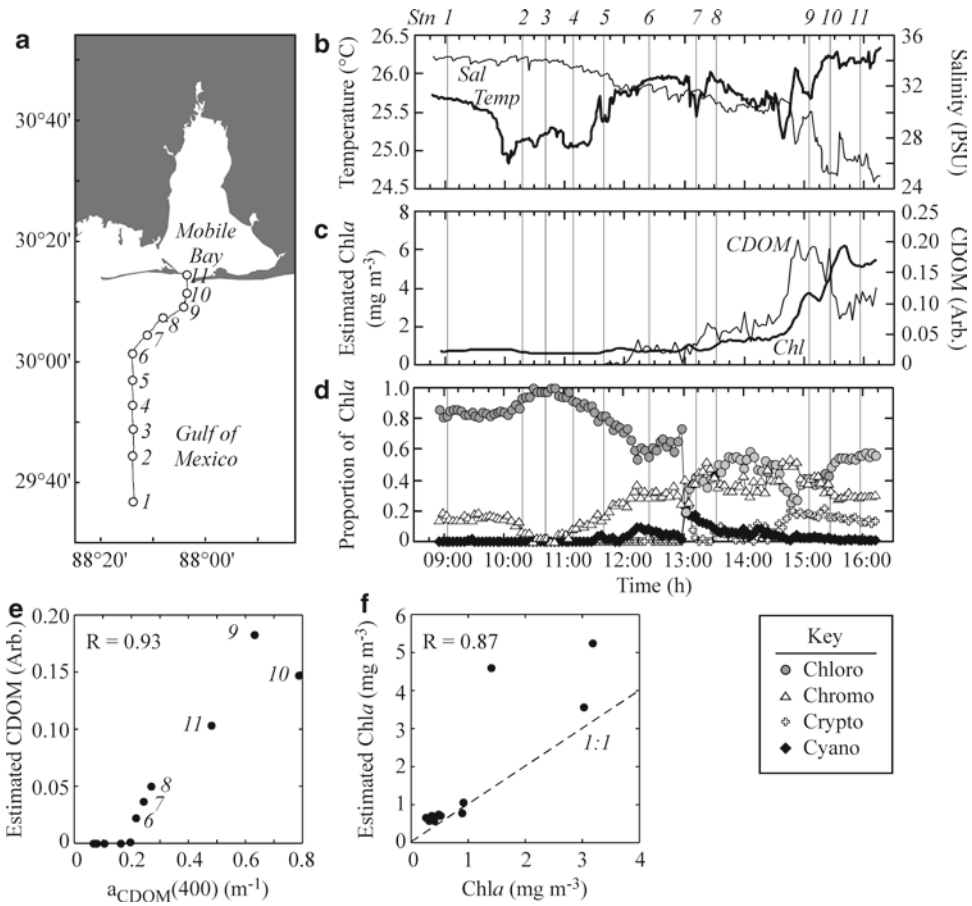


**Fig. 18** Variation in physical and optical parameters along a coastal transect. (**a**) Cruise-track offshore from Mobile Bay. Latitude and longitude are in °N and °W. Numbers correspond to stations where discrete samples were taken for ground-truthing. (**b**) Along-track variation in salinity and temperature measured in flow-through mode with a YSI MIDAS CT 6700 sensor. Vertical lines refer to the sampling stations. (**c**) Along-track variation in CDOM and Chl*a* concentrations measured in flow-through mode with *bbe* Moldaenke's AOA. (**d**) Along-track variation in the abundance of four taxonomic groups measured in flow-through mode with *bbe* Moldaenke's AOA. Data are given as the proportion of total estimated Chl*a*. The instrument was calibrated with the chlorophyte *Dunaliella tertiolecta,* the chromophyte (diatom) *Thalassiosira pseudonana,* the cryptophyte *Rhodomonas lens* and the cyanobacterium *Synechococcus bacillaris* (Fig. 5). The key to symbols is below the panel. (**e**) Estimates of CDOM made with the AOA as a function of measured CDOM absorption. Station numbers are indicated beside the data. (**f**) Estimates of Chl*a* made with the AOA as a function of measured concentrations

mouth of Mobile Bay, reflecting the typical variation along the salinity gradient within the bay (cf. Fig 13, 17). Features in the CDOM estimate were coherent with the salinity record, although CDOM was below the AOA's limit of detection at Stations 1–5 (Fig. 18c). Estimates of Chl*a* varied by more than an order of magnitude along the cruise-track and also showed coherence with features in the physical hydrography, although these were less pronounced than the CDOM record.

The AOA's taxonomic classification is shown in Fig. 18d. The data have been normalized to Chl*a* to emphasize the differences in the assigned classification rather than differences in apparent biomass. The classification was dominated by chlorophytes between Stations 1 and 6, with a minor contribution by chromophytes and negligible contributions of cryptophytes and cyanobacteria. Enhanced dominance of the classification by chlorophytes is evident at Stations 2–4, which are hydrographically distinct, based on their temperature regime (Fig. 18a). The classification shows a major discontinuity between Stations 7 and 8, coherent with a disjunction in the salinity record. Stations 7–11 were classified with higher ratios of chromophytes to chlorophytes, and with an increasing

contribution of cryptophytes at Stations 9–11. There was a peak in phytoplankton classified as cyanobacteria at Stations 7 and 8, in and landward of the discontinuity in the salinity record.

The AOA's estimates of CDOM and Chl*a* relative to analytical measures on the discrete samples are shown in Fig. 18e and f. The AOA's estimates of CDOM were highly correlated with $a_{CDOM}(400)$ for estimates above the apparent limit of detection of c. 0.2 $m^{-1}$. Although Pearson's R for these six samples was 0.93, there are obvious differences in the ratio of observed to expected values in the three stations closest to Mobile Bay. These were drawn from hydrographically-distinct samples (Fig. 18b, c) and presumably reflect differences in the quantum yield of CDOM in samples from distinct sources (Del Castillo et al. 1999; Chen et al. 2007). The AOA's estimates of Chl*a* were significantly correlated ($p < 0.05$, $R = 0.87$) with HPLC-based measurements. For the more appropriate correlation between log-transformed data, which conform to the requirement of a normal distribution, $R = 0.91$. There was a 3.7*x* range in the ratio of estimated to observed Chl*a*, suggesting that the correlation was due as much of the 12.5*x* dynamic range in Chl*a* as to the implicit assumption of constant $F^{Chl}$.

The HPLC data were used to classify the taxonomic structure by MDS ordination and cluster analysis. The pigments that present were chlorophylls *b*, $c_2$ and $c_3$, prasinoxanthin, fucoxanthin and its derivatives 19′-butanoyloxyfucoxanthin and 19′-hexanoyloxyfucoxanthin, peridinin, gyroxanthin di-ester, diadinoxanthin and diatoxanthin, alloxanthin and zeaxanthin and the ubiquitous pigments Chl*a* and α- plus β-carotene. Diadinoxanthin and diatoxanthin were grouped, as samples were not filtered rapidly enough to preserve the *in situ* level of de-epoxidation and as the duration of the AOA's interrogation allows some relaxation of NPQ (Fig. 12b). Although Chl*b* was detected at all sites and prasinoxanthin (a marker for a subset of the prasinophytes) was found at all but Stations 2–4, lutein was above the limit of detection in only one sample (Station 9).

Because the objective was to compare the pigment-based community structure with the AOA's classification (i.e., removing the effect of varying biomass, cf. Fig. 18d), concentrations of pigments that could be used to classify phytoplankton at the class level or better (i.e. all but α- plus β-carotene) were expressed as ratios to Chl*a*. Pigments were standardized and square-root transformed to reduce the influence of abundant forms on the analysis. The matrix of pairwise Bray-Curtis similarity coefficients was grouped by cluster analysis. Ordination of the matrix in a MDS plot shows the existence of 3 well-supported groups (Fig. 19a). These were the three stations closest to Mobile Bay (Stations 9–11), 3 stations in a hydrographically-distinct offshore region (Stations 2–4, see Fig. 18b), and the stations in the mid-section of the transect plus that furthest from land (Stations 1 and 5–8). The AOA's classifications were treated in a similar fashion, standardized to Chl*a* and square-root transformed, prior to cluster analysis and ordination. The analysis shows the existence of two dispersed clusters, containing 5 well-supported sub-groups (Fig. 19b). The two main clusters encompass the offshore and nearshore sites (Stations 1–5 vs 6–11). Two of the clusters, A and E (Fig. 19b), correspond to Clusters I (Stations 2–4) and III (Stations 9–11) in the pigment data (Fig. 18b). The remaining cluster in the analysis of pigments, Cluster II, corresponded to Clusters B–D in the AOA data, which were distributed between the offshore and onshore groupings (Fig. 18b).

The mean pigment ratios of Clusters I–III, based on the pigment data, are compared with Clusters A–E, based on the AOA classification in Fig. 19c. Although there are strong trends in zeaxanthin, cyanobacteria were only a minor component of the AOA's classification. This may reflect the relatively high zeaxanthin:Chl*a* ratios in cyanobacteria (e.g., 0.4–1.8 g $g^{-1}$ in *Synechococcus* WH7803, Kana and Glibert 1987; Kana et al. 1988) or might reflect mis-classification of PE-rich forms based on the calibration with a PC-rich isolate. The latter seems unlikely, as PE-rich forms would likely be classified as a mixture of cryptophytes and cyanobacteria (cf. the rhodophyte *Porphyridium cruentum*, Fig. 5) and the estimates of cryptophytes were low. The latter were broadly consistent with the distributions of alloxanthin (Fig. 19c). Alloxanthin is not a particularly useful index for comparison with the AOA's cryptophyte signature, which is weighted heavily by PE, because the PE:alloxanthin ratio is highly variable, as shown earlier for *Rhodomonas lens* (Fig. 8k).

Although the AOA's classifications were dominated by chlorophytes (Fig. 18d, 19c), the accessory pigments contained high levels of chlorophylls and carotenoids associated with multiple classes of chromophytes. The absolute concentrations should be interpreted with

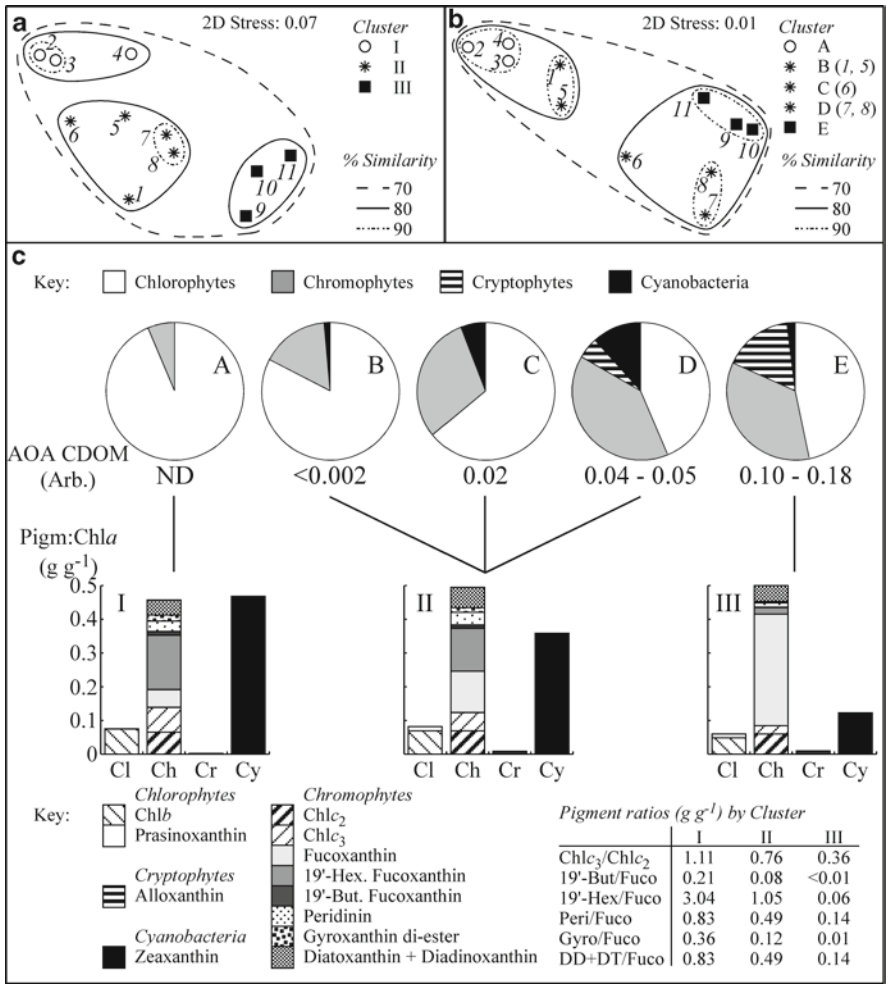


**Fig. 19** (**a**) Multidimensional scaling plot of the pigment composition from Stations 1–11 (see Fig. 18a). Data were normalized to Chl*a*, standardized and square-root transformed. Similarities based on cluster analysis are overlaid on the symbols. (**b**) Multidimensional scaling plot of the AOA classification from the same stations. Data were normalized to Chl*a*, standardized and square-root transformed. Similarities based on cluster analysis are overlaid on the symbols. The symbols are those from (**a**). (**c**) Comparison of the mean proportions of taxa in Clusters **a–e** from (**b**), upper row, and the pigment ratios in the corresponding Clusters I – III from (**a**), lower row. The keys are above and below the clusters. The connecting lines indicate correspondence. Columns within each histogram correspond to diagnostic pigments for chlorophytes (Cl), chromophytes (Ch), cryptophytes (Cr) and cyanobacteria (Cy). Ratios of pigments within the chromophytes in Clusters I – III are tabulated at the lower right

caution as the characterisitic ratios to Chl*a* vary widely, but the types of chromophytes which can be inferred from the pigment data could lead to a bias in their classification by the AOA. The presence of Chl$c_3$, 19′-butanoyloxyfucoxanthin, 19′-hexanoyloxyfucoxanthin and gyroxanthin di-ester are indicative of fucoxanthin-containing dinoflagellates in the family Kareniaceae (Millie et al. 1997), although the pigments are found individually in both the pelagophytes and prymnesiophytes (Bidigare 1989; Jeffrey and Vesk 1997). *Karenia brevis* and *Karlodinium veneficum*, two bloom-forming members of the Kareniaceae, are frequently observed at the study sites. Their presence was not confirmed by microscopy, but the concentrations of gyroxanthin di-ester (<5–17 pg $L^{-1}$) suggest densities of ca. 60 cells $L^{-1}$ of *Karenia* (Richardson and Pinckney 2004). The presence of peridinin is diagnostic of dinoflagellates (Jeffrey and Vesk 1997). The presence of high fucoxanthin levels relative to the other chromophyte pigments in Cluster III (Fig 19c) is consistent with the dominance by diatoms. As we have shown (Fig. 6b), some chromophytes are classified by

the AOA as a mixture of chlorophytes and chromophytes, notably the two prymnesiophytes and two members of the Kareniaceae *(Karenia brevis* and *Karlodinium veneficum*). The apparent dominance by chlorophytes may therefore be due in part to shifts within the chromophytes as well as changes in the abundance of chlorophytes.

We can test this by comparing the structure of the matrices based on the pigment and AOA data, using the BEST test in PRIMER-E (Clarke et al. 2008). The test ranks the similarity coefficients within each matrix and then tests for correlation between the two ranked arrays. (Note that it works from the individual samples, not from aggregated data, so is not biased by groupings defined by the cluster analysis in Fig. 19.) After ranking, it is possible to use permutative testing, creating new similarity matrices of all combinations of single through multiple input parameters. In this case, matrices based on single pigments to combinations of up to 5 pigments were compared with the matrix of AOA classifications. The test was significant at p = 0.001, indicating a vanishingly-low probability that the AOA's classification resembled the pigment classification (Fig. 19a, b) through random chance. Examination of the correlations between subsets of the pigment data and the AOA classification (Table 3) shows that the best agreement (R = 0.802) was found using five pigments that are distributed between and within the chlorophytes and chromophytes (Chl$c_2$, Chl$c_3$, fucoxanthin, 19′-hexanoyloxyfucoxanthin and prasinoxanthin – note that Chl*b* was not one of these and that prasinoxanthin is present only in a subset of the Chl*b*-containing chlorophytes). The high correlation shows that the AOA is sensitive to changes in the community structure but also suggests that the classification is driven in part by shifts within the chromophyte community. The predominance of Chl$c_3$ and 19′-hexanoyloxyfucoxanthin within the best fits with permutative testing, and the 59*x* change in the ratio of 19′-hexanoyloxyfucoxanthin to fucoxanthin between Clusters I–III (Fig. 19c) are consistent with varying levels of prymnesiophyes (which may be classified as chlorophyte/chromophyte mixtures, Fig. 6b) vs diatoms driving much of the variability in classification. The higher proportion of prymnesiophytes offshore might therefore be responsible for the higher apparent abundance of chlorophytes in Cluster A (Stations 2–4). Although the ratios of 19′-butanoyloxyfucoxanthin and gyroxanthin

**Table 3** Results of BEST test of PRIMER-E (Clarke et al. 2008) comparing pigment ratios, and pigment ratios plus the AOA's estimate of CDOM to the pair-wise similarity matrix of the AOA's taxonomic classification. Both sets of comparisons were significant (p ≤ 0.001). Permutation testing of successive subsets of the parameters was conducted to isolate those with highest explanatory power, using Spearman's R for the rank correlation method. The parameters with the highest R value for N factors (single and combinations of 2–5) are shown for each test. The combination with the highest R value in each test is in bold. Abbreviations: Prasino, prasinoxanthin, 19′-Hex, 19′-hexanoyloxyfucoxanthin; Fuco, fucoxanthin; DD+DT, sum of diadinoxanthin and diatoxanthin

| Inputs | N | R | Parameters |
|---|---|---|---|
| *Pigments* | 1 | 0.606 | Chl$c_3$ |
| | | 0.595 | 19′-Hex |
| | 2 | 0.749 | Prasino, |
| | | 0.682 | 19′-Hex19′-Hex, Fuco |
| | 3 | 0.785 | Chl$c_3$, Prasino, 19′-Hex |
| | | 0.779 | Prasino, 19′-Hex, Fuco |
| | 4 | 0.801 | Chl$c_2$, Chl$c_3$, Prasino, 19′-Hex |
| | | 0.796 | Chl$c_3$, Prasino, 19′-Hex, Fuco |
| | **5** | **0.802** | **Chl$c_2$, Chl$c_3$, Fuco, Prasino, 19′-Hex** |
| | | 0.778 | Chl$c_3$, Prasino, 19′-Hex, Fuco, DDT+DT |
| *Pigments, AOA CDOM* | 1 | 0.712 | CDOM |
| | | 0.606 | Chl$c_3$ |
| | 2 | 0.874 | Chl$c_2$, CDOM |
| | | 0.869 | Fuco, CDOM |
| | 3 | 0.855 | Prasino, 19′-Hex, CDOM |
| | | 0.854 | Chl$c_2$, Fuco, CDOM |
| | **4** | **0.885** | **Chl$c_2$, Prasino, 19′-Hex, CDOM** |
| | | 0.876 | Chl$c_3$, Prasino, 19′-Hex, CDOM |
| | 5 | 0.879 | Chl$c_2$, Chl$c_3$, Prasino, 19′-Hex, CDOM |
| | | 0.872 | Chl$c_3$, Fuco, Prasino, 19′-Hex, CDOM |

di-ester to fucoxanthin varied by 51*x* and 28*x* between Clusters I and III (Fig. 19c), neither had any significant correlation with the changes in the AOA's classification (Table 3). It is unlikely therefore that the pattern was due to shifts in the relative abundance of *Karenia* or *Karlodinium*.

Although the comparison of the pigment and classification matrices shows a highly significant relationship and high correlation, it offers little insight into the division of pigment Cluster II between classification Clusters B–D (Fig. 19c). Cursory inspection of the classification clusters shows that the most significant division, between Clusters A, B *vs* C–E, follows the gradient in CDOM, which was below the AOA's limit of detection in the former but detectable in the latter. The division of pigment Cluster II between classification Clusters B–D also follows the gradient in CDOM, with progressively lower proportions of chromophytes occurring as CDOM increases. The trend might reflect covariance, as a trend in decreasing nutrient availability and increasing water clarity as CDOM declines with distance from land. However, the lab-based tests predict that this would result in identification of higher proportions of chlorophytes and lower proportions of cryptophytes offshore as cryptophytes become progressively more nutrient- and light-stressed (Fig. 10c). This is the opposite of what we observe in Clusters B–D. Instead, the data are consistent with the effects of optical interference. The AOA classifications are corrected for interference by CDOM but we did not calibrate the instrument with local CDOM. Under-correction for CDOM interference would cause an anti-clockwise rotation in the Norm SFS (Fig. 14a–d) and cause an under-estimate of chlorophytes and an over-estimate of cyanobacteria and cryptophytes. This is consistent with the trends in these taxa with CDOM between Clusters B and D (Fig. 19c). Under-correction could cause an increase in chromophytes through mis-classification of chlorophytes (be they true chlorophytes or inaccurately assigned chromophytes) or an underestimate through mis-classification of chromophytes (Fig. 14e). The increasing trend in chromophytes with CDOM suggests the former is predominant. The trends evident within Clusters B–D are consistent with lower and higher interference by CDOM in Clusters A and E (Fig. 19c), although the pigment ratios are different.

We can test for the effect of the CDOM correction by including the AOA's estimate of CDOM in the pigment matrix and repeating the permutative tests. The permutative tests show that the estimate of CDOM has higher explanatory power as a single factor than any pigment (Table 3) and is consistently present in the highest-ranked combinations of 2–5 input parameters. When it is included, the correlation coefficients between the [pigment + CDOM] matrix and the AOA classification matrix are consistently higher than the coefficients for the pigment matrix alone (Table 3). The optimum occurs with 4 parameters: the ratios of Chl$c_2$, prasinoxanthin, and 19′-hexanoyloxyfucoxanthin to Chl*a*, and CDOM. Although the most highly-ranked pigments are consistent between both sets of comparisons, the correlation is higher when CDOM is included: R = 0.885 *vs* 0.802. The best correlation occurred with 4 inputs, rather than 5, indicating that forcing inclusion of the variance structure associated with the fifth variable reduced the goodness of fit. The correlation with 5 inputs was still higher than when CDOM was not included. The results indicate that the bias reflects inadequate correction for the CDOM interference. We did not calibrate the instrument with locally-occurring CDOM and infer that the classification was under-corrected, and that shifts in the classification within Cluster II, as well as between Clusters I–III, reflect incomplete correction for the effects of background optical interference recognition of the SFS.

These patterns are broadly consistent with differences in classification by SFS vs pigment matrices reported by See et al. (2005), who also conducted a study in the Gulf of Mexico, using a Fluoroprobe (*bbe* Moldaenke). This instrument differs from the AOA in having an open interrogation volume, and would therefore be more susceptible to variation in $F^{Chl}$ due to actinic irradiance when used *in situ* (Fig. 15–16). See et al. (2005) used the Fluoroprobe on shipboard, using a ca. 1-min interrogation of surface samples that were shrouded to prevent actinic interference, so it is not clear to what degree quenching would have relaxed. It was calibrated on a slightly different suite of phytoplankton than we used (the diatom *Thalassiosira weissflogii* rather than *T. pseudonana*, and the cyanobacterium *Synechococcus sp*. rather than *S. bacillaris*). Pigments were used to construct taxonomic classifications using CHEMTAX (Mackey et al. 1996). The results were similar to those we report here: the SFS-based classifications showed dominance by chlorophytes (57–81%), with substantial contributions from cryptophytes (13–20%), while the pigment-based classification

showed dominance by diatoms and dinoflagellates (61–95%), with negligible contributions by cryptophytes (0–2%) except at one station (25%). Cyanobacteria were not detected with the Fluoroprobe and were estimated at only 0–6% of the population by CHEMTAX. It is not clear if the *Synechococcus sp*. used to calibrate the Fluoroprobe was a PE- or PC-rich strain but the complete absence of cyanobacteria from the SFS classification suggests that they were not responsible for the overestimate of cryptophytes. We would predict classification as mixed cyanobacteria/cryptophytes if the instrument were calibrated with PC-rich strain of *Synechococcus* and challenged with PE-rich strains (cf. *Porphyridium*, Fig. 5b and c) and mixed cyanobacteria/chlorophytes if it were calibrated with a PE-rich strain and challenged with PC-rich ones. (This assumption is based on re-alignment of the calibration tetrahedron in Fig. 5b so that the cyanobacterial apex is defined by PE-rich *Porphyridium* and the PC-rich *Synechoccocus* becomes the unknown sample.) The results reported by See and co-workers (See et al. 2005) are consistent with chromophytes that were mis-classified as either chlorophyte/chromophyte or chromophyte/cryptophyte mixtures (cf. Fig. 6a, b). As two of the five stations occupied were adjacent to estuaries, there may also have been interference by CDOM causing some fraction of chromophytes to be classified as cryptophytes.

## 6 Conclusion

Taxonomic classification by SFS is subject to bias in the signatures from inter- and intra-specific variation in the shape of signatures and in $F^{Chl}$, and in the relationship between fluorescence intensity and Chl*a*. These observations are well-recognized, as noted by Poryvkina et al. (2000), "all attempts to provide universal calibration of phytoplankton fluorescence have been doomed to failure". Beyond variability in the shape and magnitude of the SFS, the effect of interfering chromophores (CDOM and other materials that absorb or scatter light) must also be considered. Even so, like other researchers using the method, we find that relationships between fluorescence and Chl*a* are robust, provided that the dynamic range of the signal is large enough, and that there is qualitative agreement between classification by SFS and other analytical methods. We have demonstrated in field tests that, although the accuracy of identification from SFS is subject to (somewhat predictable) bias, it is sensitive to changes in community structure: the inaccuracy is inherent in the use of unique and invariant classification algorithms, not in the fluorescence method *per se*. Because it is capable of monitoring communities continuously and at relatively minor cost, the SFS approach is well-suited as a trigger for adaptive sampling, as a low-level form of screening that can optimize the use of more accurate but more expensive or laborious analyses. In closing, we reiterate the observation made by John Cullen, an early advocate for the use of fluorescence in studying phytoplankton (and a graduate advisor to both HM and TR), that, "we may not know exactly what we are measuring, but the patterns observed are too strong to ignore" (Cullen and Renger 1979).

**Acknowledgements** We thank Geir Johnsen and an anonymous reviewer for comments that improved this work. We thank Adrienne Stutes, Andy Canion, Alison Rellinger, Preston Kendrick and Emily Goldman for assistance in field sampling and lab work. HLM was supported by the US National Atmospheric and Oceanographic Administration's Cooperative Institute for Coastal and Estuarine Environmental Technology (Grant number NA06NOS4190167). HLM acknowledges support for supplementary fieldwork from the US EPA (Grant numbers X-93190401 and R-83065101-1-6) and US Department of Commerce (Grant number NA17FZ2602-A3-08), administered through the Alabama Center for Estuarine Studies and the Alabama Oyster Reef Restoration Program. TLR acknowledges support from the US National Science Foundation (Grant numbers OCE06234001 and CBET0606940) and the South Carolina Sea Grant Consortium (Grant number P/M-2J-V410).

## References

Aberle N, Beutler M, Moldaenke C, Wiltshire KH (2006) 'Spectral fingerprinting' for specific algal groups on sediments *in situ*: a new sensor. Arch Hydrobiol 167:575–592

Ahn Y-H, Bricaud A, Morel A (1992) Light backscattering efficiency and related properties of some phytoplankters. Deep Sea Res 39:1835–1855

Allen JF (2002) Plastoquinone redox control of chloroplast thylakoid protein phosphorylation and distribution of excitation energy between photosystems: discovery, background, implications. Photosynth Res 73:139–148

Allen JF, Mullineaux CW (2004) Probing the mechanism of state transitions in oxygenic photosynthesis by chlorophyll fluorescence spectroscopy, kinetics and imaging. In: Papageorgiou GC, Govindjee (eds) Chlorophyll *a* fluorescence: a signature of photosynthesis. Springer, Dordrecht, pp 447–461

Alpine AE, Cloern JE (1985) Differences in *in vivo* fluorescence yield between three phytoplankton size classes. J Plankt Res 7:381–390

Andersen RA, Bidigare RR, Keller MD, Latasa M (1996) A comparison of HPLC pigment signatures and electron microscopic observations for oligotrophic waters of the North Atlantic and Pacific Oceans. Deep Sea Res 43:517–537

Anning T, Harris G, Geider RJ (2001) Thermal acclimation in the marine diatom *Chaetoceros calcitrans* (Bacillariophyceae). Eur J Phycol 36:233–241

Apt KE, Collier JL, Grossman AR (1995) Evolution of the phycobiliproteins. J Mol Biol 248:79–96

Arsalane W, Rousseau B, Duval J-C (1994) Influence of the pool size of the xanthophyll cycle on the effects of light stress in a diatom: competition between photoprotection and photoinhibition. Biochem Photobiol 60:237–243

Babichenko S, Leeben A, Poryvkina L, van der Wagt R, de Vos F (1994) Fluorescent screening of phytoplankton and organic compounds in sea water. J Environ Monit 2:378–383

Babichenko S, Kaitala S, Leeben A, Poryvkina L, Seppala J (1999) Phytoplankton pigments and dissolved organic matter distribution in the Gulf of Riga. J Mar Syst 23:69–82

Babichenko S, Leeben A, Poryvkina L, van der Wagt R, de Voss F (2000) Fluorescent screening of phytoplankton and organic compounds in sea water. J Environ Monit 2:378–383

Babin M (2008) Phytoplankton fluorescence: theory, current literature and *in situ* measurement. In: Babin M, Roesler CS, Cullen JJ (eds) Real-time coastal observing systems for ecosystem dynamics and harmful algal blooms. UNESCO Publishing, Paris, pp 237–280

Beeler SooHoo J, Kiefer DA, Collins DJ, McDermid IS (1986) *In vivo* fluorescence excitation and absorption spectra of marine phytoplankton: I. Taxonomic characteristics and responses to photoadaptation. Plankton Res 8:197–214

Benson EE, Cobb AH (1981) Pigment/protein complexes of the intertidal alga *Codium fragile* (Suringar) Hariot. New Phytol 88:627–632

Beutler M, Wiltshire KH, Meyer B, Moldaenke C, Lüring C, Meyerhöfer M, Hansen U-P, Dau H (2002) A fluorometric method for the differentiation of algal populations *in vivo* and *in situ*. Photosynth Res 72:39–53

Beutler M, Wiltshire KH, Arp M, Kruse J, Reineke C, Moldaenke C, Hansen U-P (2003) Reduced model of the fluorescence from the cyanobacterial photosynthetic apparatus designed for the *in situ* detection of cyanobacteria. Biochim Biophys Acta 1604:33–46

Beutler M, Wiltshire KH, Reineke C, Hansen U-P (2004) Algorithms and practical fluorescence models of the photosynthetic apparatus of red cyanobacteria and Cryptophyta designed for the fluorescence detection of red cyanobacteria and cryptophytes. Aquat Microb Ecol 35:115–129

Bidigare RR (1989) Photosynthetic pigment composition of the brown tide alga: unique chlorophyll and carotenoid derivatives. In: Cosper EM, Bricelj VM, Carpenter EJ (eds) Novel phytoplankton blooms: causes and impacts of recurrent brown tides and other unusual blooms. Springer, Berlin, pp 57–76

Bidigare RR, Ondrusek ME, Morrow JH, Kiefer DA (1990) *In vivo* absorption properties of algal pigments. SPIE 1302:290–302

Bodemer U (2004) Variability of phycobiliproteins in cyanobacteria detected by delayed fluorescence excitation spectroscopy and its relevance for determination of phytoplankton composition of natural water samples. J Plankton Res 26:1147–1162

Bouman H, Platt T, Sathyendranath S, Stuart V (2005) Dependence of light-saturated photosynthesis on temperature and community structure. Deep Sea Res 52:1284–1299

Bricaud A, Claustre H, Ras J, Oubelkheir K (2004) Natural variability of phytoplanktonic absorption in oceanic waters: Influence of the size structure of algal populations. J Geophys Res 109:C11010

Buiteveld H, Hakvoort JHH, Donze M (1994) The optical properties of pure water. SPIE, Ocean Optics XIII

Burger-Wiersma T, Post AF (1989) Functional analysis of the photosynthetic appratus of *Prochlorothrix hollandica* (Prochlorales), a Chlorophyll *b* containing procaryote. Plant Physiol 91:770–774

Butler WL, Hopkins DW (1970a) An analysis of fourth derivative spectra. Photochem Photobiol 12:451–456

Butler WL, Hopkins DW (1970b) Higher derivative analysis of complex absorption spectra. Photochem Photobiol 12:439–450

Campbell D, Oquist G (1996) Predicting light acclimation in cyanobacteria from nonphotochemical quenching of photosystem II fluorescence, which reflects state transitions in these organisms. Plant Physiol 111:1293–1298

Casper-Lindley C, Björkman O (1998) Fluorescence quenching in four unicellular algae with different light-harvesting and xanthophyll-cycle pigments. Photosynth Res 56:277–289

Wit CDv-D, Doust AB, van Stokkurn LHM, Dekker JP, Wilk KE, Curmi PMG, van Grondelle R (2008) Phycocyanin sensitizes both photosystem I and photosystem II in cryptophyte *Chroomonas* CCMP270 cells. Biophys J 94:2423–2433

Chekalyuk AM, Hafez M (2008) Advanced laser fluorometry of natural aquatic environments. Limnol Oceanogr Methods 6: 591–609

Chekalyuk AM, Hoge FE, Wright CW, Swift RN, Yungel JK (2000) Airborne test of laser pump-and-probe technique for assessment of phytoplankton photochemical characteristics. Photosynth Res 66:45–56

Chen ZQ, Hu CM, Comny RN, Muller-Karger F, Swarzenski P (2007) Colored dissolved organic matter in Tampa Bay, Florida. Mar Chem 104:98–109

Chisholm SW, Frankel SL, Goericke R, Olson RJ, Palenik B, Waterbury JB, West-Johnsrud L, Zettler ER (1992) *Prochlorococcus marinus* nov. gen. nov. sp.: An oxytrophic procaryote containing divinyl-chlorophyll b. Arch Microbiol 157:297–300

Clarke KR, Warwicke RM (2001) Change in marine communities: an approach to statistical analysis and interpretation. Plymouth, PRIMER-E

Clarke KR, Somerfield PJ, Gorley RN (2008) Testing of null hypotheses in exploratory community analyses: similarity profiles and biota-environment linkage. J Exp Mar Biol Ecol 366:56–69

Collier JL, Herbert SK, Fork DC, Grossman AR (1993) Changes in the cynaobacterial photosynthetic apparatus during acclimation to macronutrient deprivation. Photosynth Res 42:173–183

Cowles TJ, Desiderio RA, Neuer S (1993) *In situ* characterization of phytoplankton from vertical profiles of fluorescence emission spectra. Mar Biol 115:217–222

Cullen JJ, Renger EH (1979) Continuous measurement of the DCMU-induced fluorescence response of natural phytoplankton populations. Mar Biol 53:13–20

Cullen JJ, Yang X, MacIntyre HL (1992) Nutrient limitation and marine photosynthesis. In: Falkowski PG, Woodhead AD (eds) Primary productivity and biogeochemical cycles in the sea. Plenum Press, New York, pp 69–88

Del Castillo CE, Coble PG, Morell JM, López JM, Corredor JE (1999) Analysis of the optical properties of the Orinoco River plume by absorption and fluorescence spectroscopy. Mar Chem 66:35–51

Demmig-Adams B (1990) Carotenoids and photoprotection in plants: a role for xanthophyll zeaxanthin. Biochim Biophys Acta 1020:1–24

Desiderio RA, Moore CC, Lantz C, Cowles TJ (1997) Multiple excitation fluorometer for *in situ* oceanographic applications. Appl Opt 36:1289–1296

Dickinson DE, Bearman G, Tille S, Lansford R, Fraser SE (2001) Multi-spectral imaging and linear unmixing add a whole new dimension to laser scanning fluorescence microscopy. BioTechniques 31:1272–1276

Falkowski PG, Raven JA (2007) Aquatic photosynthesis. Blackwell Science, Malden

Falkowski PG, Kolber Z, Fujita Y (1988) Effects of redox state on the dynamics of Photosystem II during steady-state photosynthesis in eucaryotic algae. Biochim Biophys Acta 933:432–443

Fawley MW, Lee CM (1990) Pigment composition of the scaly green flagellate *Mesostigma viridae* (Micromonadophyceae) is similar to that of the siphonous green alga *Bryopsis plumosa* (Ulvophyceae). J Phycol 26:666–670

Frank HA, Chynwat V, Desamero RZB, Farhoosh R, Erikson J, Bautista J (1997) On the photophysics and photochemical propoerties of carotenoids and their role as light-haresting pigments in photosynthesis. PureAppl Chem 69:2117–2124

Gaevsky NA, Kolmakov VI, Anishchenko OV, Gorbaneva TB (2005) Using DCMU-fluorescence method for the identification of dominant phytoplankton groups. J Appl Phycol 17:483–494

Gallegos CL, Neale PJ (2002) Partitioning spectral absorption in case 2 waters: discrimination of dissolved and particulate components. Appl Opt 41:4220–4233

Gantt E (1996) Pigment protein complexes and the concept of the photosynthetic unit: chlorophyll complexes and phycobilisomes. Photosynth Res 48:47–53

Gantt E, Lipschultz CA, Grabowski J, Zimmerman BK (1979) Phycobilisomes from blue-green and red algae. Plant Physiol 63:615–620

Garcia-Mendoza E, Matthijs HCP, Schubert H, Mur LR (2002) Non-photochemical quenching of chlorophyll fluorescence in *Chlorella fusca* acclimated to constant and dynamic light conditions. Photosynth Res 74:303–315

Geider RJ, MacIntyre HL, Kana TM (1997) Dynamic model of phytoplankton growth and acclimation: responses of the balanced growth rate and the chlorophyll *a*: carbon ratio to light, nutrient-limitation and temperature. Mar Ecol Prog Ser 148:187–200

Geider RJ, MacIntyre HL, Graziano LM, McKay RML (1998a) Responses of the photosynthetic apparatus of *Dunaliella teriolecta* (Chlorophyceae) to nitrogen and phosphorus limitation. Eur J Phycol 33:315–332

Geider RJ, MacIntyre HL, Kana TM (1998b) A dynamic regulatory model of phytoplanktonic acclimation to light, nutrients and temperature. Limnol Oceanogr 43:679–694

Genty B, Briantais J-M, Baker NR (1989) The relationship between the quantum yield of photosynthetic electron transport and quenching of chlorophyll fluorescence. Biochim Biophys Acta 990:87–92

Genty B, Harbinson J, Briatais J-M, Baker NR (1990) The relationship between non-photochemical quenching of chlorophyll fluorescence and the rate of photosystem 2 photochemistry in leaves. Photosynth Res 25:249–257

Gerhardt V, Balode M (1998) Delayed fluorescence excitation spectroscopy: a method for automatic determination of phytoplankton composition of freshwaters and sediments (interstitial) and of algal composition of benthos. Limnologica 28:313–322

Goericke R, Montoya JP (1998) Estimating the contribution of microalgal taxa to chlorophyll *a* in the field – variations of pigment ratios under nutrient- and light-limited growth. Mar Ecol Prog Ser 169:97–112

Goericke R, Welschmeyer NA (1992a) Pigment turnover in the marine diatom *Thalassiosira weissflogii*. I. The $^{14}CO_2$-labeling kinetics of chlorophyll *a*. J Phycol 28:498–507

Goericke R, Welschmeyer NA (1992b) Pigment turnover in the marine diatom *Thalassiosira weissflogii*. II. The $^{14}CO_2$-labeling kinetics of carotenoids. J Phycol 28:507–517

Goss R, Lepetit B, Wilhelm C (2006) Evidence for a rebinding of antheraxanthin to the light-harvesting complex during the epoxidation reaction of the violaxanthin cycle. J Plant Physiol 163:585–590

Gregg WW, Carder KL (1990) A simple spectral solar irradiance model for cloudless maritime atmospheres. Limnol Oceanogr 35:1657–1675

Gregor J, Geris R, Marsálek B, Hetesa J, Marvan P (2005) *In situ* quantification of phytoplankton in reservoirs using a submersible spectrofluorometer. Hydrobiologia 548:141–151

Grossman AR, Schefer MR, Chiang GG, Collier JL (1993) The responses of cyanobacteria to environmental conditions: light and nutrients. In: Bryant DA (ed) The molecular biology of cyanobacteria. Kluwer, The Netherlands, pp 641–675

Hammer A, Schumann R, Schubert H (2002) Light and temperature acclimation of *Rhodomonas salina* (Cryptophyceae): photosynthetic performance. Aquat Microb Ecol 29:287–296

Haxo FT, Blinks LR (1950) Photosynthetic action spectra of marine algae. J Gen Physiol 33:389–422

Henriksen P, Riemann B, Kaas H, Sorensen H, Sorensen H (2002) Effects of nutrient-limitation and irradiance on marine phytoplankton pigments. J Plankt Res 24:835–858

Hilton J, Rigg E, Jaworski G (1988) *In vivo* algal fluorescence, spectral change due to light intensity changes and the automatic characterization of algae. Freshw Biol 21:375–382

Hilton J, Rigg E, Jaworski G (1989) Algal identification using *in vivo* fluorescence spectra. J Plankt Res 11:65–74

Hoef-Emden K (2008) Molecular phylogeny of phycocyanin-containing cryptophytes: Evolution of biliproteins and geographical distribution. J Phycol 44:985–993

Hooks CE, Bidigare RR, Keller MD, Guillard RRL (1988) Coccoid eukaryotic ultraplankters with four different HPLC pigment signatures. J Phycol 24:571–580

Itoh S, Sugiura K (2004) Fluorescence of photosystem I. In: Papageorgiou GC, Govindjee (eds) Chlorophyll *a* fluores-

cence: a signature of photosynthesis. Springer, Dordrecht, pp 231–250
Jackson DA, Somers KM (1991) The spectre of 'spurious' correlations. Oecologia 86:147–151
Jakob T, Schreiber U, Kirschesch V, Langner U, Wilhelm C (2005) Estimation of chlorophyll content and daily primary production of the major algal groups by means of multiwavelength-excitation PAM chlorophyll fluorometry: performance and methodological limits. Photosynth Res 83:343–361
Jeffrey SW, Vesk M (1997) Introduction to marine phytoplankton and their pigment signatures. In: Jeffrey SW, Mantoura RFC, Wright SW (eds) Phytoplankton pigments in oceanography: guidelines to modern methods. UNESCO Publishing, Paris, pp 37–84
Jeffrey SW, Mantoura RFC, Wright SW (1997) Phytoplankton pigments in oceanography: guidelines to modern methods. UNESCO Publishing, Rome
Johnsen G, Sakshaug E (2007) Biooptical characteristics of PSII and PSI in 33 species (13 pigment groups) of marine phytoplankton, and the relevance for pulse-amplitude-modulated and fast-repetition-rate fluorometry. J Phycol 43:1236–1251
Johnsen G, Samset O, Granskog L, Sakshaug E (1994) *In-vivo* absorption characteristics in 10 classes of bloom-forming phytoplankton – taxonomic characteristics and responses to photoadaptation by means of discriminant and HPLC analysis. Mar Ecol Prog.Ser 105:149–157
Johnsen G, Prézelin BB, Jovine RVM (1997) Fluorescence excitation spectra and light utilization in two red tide dinoflagellates. Limnol Oceanogr 42:1166–1177
Johnson Z, Barber RT (2003) The low-light reduction in the quantum yield of photosynthesis: potential errors and biases when calculating the maximum quantum yield. Photosynth Res 75:85–95
Jovine RVM, Johnsen G, Prézelin BB (1995) Isolation of membrane bound light-haryesting-complexes from the dinoflagellates *Heterocapsa pygmaea* and *Prorocentrum minimum*. Photosynth Res 44:127–138
Kana TM, Glibert PM (1987) Effect of irradiances up to 2000 μE $m^{-2}$ $s^{-1}$ on marine *Synechococcus* WH7803 – I. Growth, pigmentation, and cell composition. Deep Sea Res 34:479–495
Kana TM, Glibert PM, Goericke R, Welschmeyer NA (1988) Zeaxanthin and β-carotene in *Synechococcus* WH7803 respond differently to irradiance. Limnol Oceanogr 33:1623–1627
Kiefer DA (1973a) Chlorophyll *a* fluorescence on marine centric diatoms: responses of chloroplasts to light and nutrient stress. Mar Biol 23:39–46
Kiefer DA (1973b) Fluorescence properties of natural phytoplankton populations. Mar Biol 22:263–269
Kieleck C, Bousquet B, Le Brun G, Cariou J, Lotrian J (2001) Laser induced fluorescence imaging: application to groups of macroalgae identification. J Phys D: Appl Phys 34:2561–2571
Kirk JTO (1994) Light and photosynthesis in aquatic ecosystems. Cambridge University Press, Cambridge
Koblizek M, Kaftan D, Nedbal L (2001) On the relationship between the non-photochemical quenching of the chlorophyll fluorescence and the Photosystem II light harvesting efficiency. A repetitive flash fluorescence induction study. Photosynth Res 68:141–152
Kolber Z, Zehr J, Falkowski P (1988) Effects of growth irradiance and nitrogen limitation on photosynthetic energy conversion in photosystem II. Plant Physiol 88:923–929
Kolbowski J, Schreiber U (1995) Computer-controlled phytoplankton analyzer based on 4-wavelengths PAM chlorophyll fluorometer. In: Mathis P (ed) Photosynthesis: from light to biosphere, vol V. Kluwer, The Netherlands, pp 825–828
Kopf U, Heinze J (1984) 2, 7-bis(diehylamino)phenazoxonium chloride as a quantum counter for emission measurements between 240 and 700 nm. Anal Chem 56:1931–1935
Krause GH, Weis E (1991) Chlorophyll fluorescence and photosynthesis: the basics. Ann Rev Plant Physiol Plant Mol Biol 42:313–349
Kromkamp JC, Forster RM (2003) The use of variable fluorescence measurements in aquatic ecosystems: differences between multiple and single turnover measuring protocols and suggested terminology. Eur J Phycol 38:103–112
Kruse O (2001) Light-induced short-term adaptation mechanisms under redox control in the PS II-LHCII supercomplex: LHC II state transitions and PSII repair cycle. Naturwissenschaften 88:284–292
Kruskopf M, Flynn KJ (2006) Chlorophyll content and fluorescence responses cannot be used to gauge reliably phytoplankton biomass, nutrient status or growth rate. New Phytol 169:525–536
Laney SR (2003) Assessing the error in photosynthetic properties determined with Fast Repetition Rate fluorometry. Limnol Oceanogr 48:2234–2242
Laney SR, Letelier R (2008) Artifacts in measurements of chlorophyll fluorescence transients, with specific application to fast repetition rate fluorometry. Limnol Oceanogr Methods 6:40–50
Latasa M (1995) Pigment composition of *Heterocapsa* sp. and *Thalassiosira weissflogii* growing in batch cultures under different irradiances. Sci Mar 59:25–37
Latasa M, Berdalet E (1994) Effect of nitrogen or phosphorus starvation on pigment composition of cultured *Heterocapsa* sp. J Plankt Res 16:83–94
Lavaud J, Strzepek RF, Kroth PG (2007) Photoproprotection capacity differs among diatoms: Possible consequences on the spatial distribution of diatoms related to fluctuations in the underwater light climate. Limnol Oceanogr 52:1188–1194
Laws EA, Bannister TT (1980) Nutrient- and light-limited growth of *Thalassiosira fluviatilis* in continuous culture, with implications for phytoplankton growth in the sea. Limnol Oceanogr 25:457–473
Lewitus AJ, Caron DA (1990) Relative effects of nitrogen or phosphorus depletion and light intensity on the pigmentation, chemical composition, and volume of *Pyrenomonas salina* (Cryptophyceae). Mar Ecol Prog Ser 61:171–181
Loftus ME, Seliger HH (1975) Some limitations of the *in vivo* fluorescence technique. Chesapeake Science 16:79–92
Lohrenz SE (2000) A novel theoretical approach to correct for pathlength amplification and variable sampling loading in measurements of particulate spectral absorption by the quantitative filter technique. J Plankt Res 22:639–657
Lorenzen CJ (1966) A method for the continuous measurement of *in vivo* chlorophyll concentration. Deep Sea Res 13:223–227
Lutz VA, Sathyendranath S, Head EJH, Li WKW (2001) Changes in the *in vivo* absorption and fluorescence excitation spectra with growth irradiance in three species of phytoplankton. J Plankt Res23:555–569

MacColl R, Guard-Friar D (1983) Phycocyanin 645. The chromophore assay of Phycocyanin 645 from the cryptomonad protozoa *Chroomonas* species. J Biol Chem 258:14327–14329

MacIntyre HL, Cullen JJ (2005) Using cultures to investigate the physiological ecology of microalgae. In: Andersen RA (ed) Algal Cultureing Techniques. Amsterdam, Elsevier, pp 287–326

MacIntyre HL, Kana TM, Geider RJ (2000) The effect of water motion on short-term rates of photosynthesis by marine phytoplankton. Trends Plant Sci 5:12–17

MacIntyre HL, Kana TM, Anning T, Geider RJ (2002) Photoacclimation of photosynthesis irradiance response curves and photosynthetic pigments in microalgae and cyanobacteria. J Phycol 38:17–38

MacIntyre HL, Lomas MW, Cornwell JC, Suggett DJ, Koch EW, Gobler CJ, Kana TM (2004) Mediation of benthic-pelagic coupling by microphytobenthos: An energy- and material-based model for initiation of blooms of *Aureococcus anophagefferens*. Harmful Algae 3:403–438

Mackey MD, Mackey DJ, Higgins HW, Wright SW (1996) CHEMTAX – a program for estimating class abundances from chemical markers: application to HPLC measurements of phytoplankton. Mar Ecol Prog Ser 144:265–283

Mazel CH (1995) Spectral measurements of fluorescence emission in Caribbean cnidarians. Mar Ecol Prog Ser 120:185–191

McLeod GC (1958) Delayed light action spectra of several algae in visible and ultraviolet light. J Gen Physiol 42:243–250

Millie DF, Om S, Kirkpatrick GJ, Johnsen G, Tester PA, Vinyard BT (1997) Detection of harmful algal blooms using photopigments and absorption signatures: a case study of the Florida red tide dinoflagellate, *Gymnodinium breve*. Limnol Oceanogr 42:1240–1251

Millie DF, Schofield OME, Kirkpatrick GJ, Johnsen G, Evens TJ (2002) Using absorbance and fluorescence spectra to discriminate microalgae. Eur J Phycol 37:313–322

Mimuro M (2005) Visualization of excitation energy transfer processes in plants and algae. In: Govindjee, Beatty JT, Gest H, Allen JF (eds) Discoveries in photosynthesis. Springer, Dordrecht, pp 171–176

Moberg L, Karlber B, Sørensen K, Källqvist T (2002) Assessment of phytoplankton class abundance using absorption spectra and chemometrics. Talanta 56:153–160

Moisan TA, Mitchell BG (1999) Photophysiological acclimation of *Phaeocystis antarctica* Karsten under light limitation. Limnol Oceanogr 44:247–258

Moore LR, Goericke R, Chisholm SW (1995) "Comparative physiology of *Synechococcus* and *Prochlorococcus*: influence of light and temperature on growth, pigments, fluorescence and absorptive properties. Mar Ecol Prog Ser 116:259–275

Morel A (1991) Optics of marine particles and marine optics. In: Demers S (ed.) Particle Analysis in Oceanography. NATO ANSI Series G 27:141–188

Mueller JL (2003) Ocean Optics Protocols for Satellite Ocean Color Sensor Validation, Revision 4, Volume IV, Err. 1. Ocean Optics Protocols for Satellite Ocean Color Sensor Validation, Revision 4. Fargion GS, Mueller JL . Goddard Space Flight Space Center, Greenbelt, Maryland, National Aeronautical and Space Administration. NASA/TM—2003-211621/Rev4-Vol.IV (ERRATUM 1)

Murphy A, Cowles T (1997) Effects of darkness on multi-excitation *in vivo* fluorescence and survival in a marine diatom. Limnol Oceanogr 42:1444–1453

Neidhardt J, Benemann JR, Zhang L, Melis A (1998) Photosystem-II repair and chloroplast recovery from irradiance stress: relationship between chronic photoinhibition, light-harvesting chlorophyll antenna size and photosynthetic productivity in *Dunaliella salina* (green algae). Photosynth Res 56:175–184

Neori A, Vernet M, Holm-Hansen O, Haxo FT (1988) Comparison of chlorophyll far-red fluorescence excitation spectra with photosynthetic oxygen action spectra for photosystem II in algae. Mar Ecol Prog Ser 44:297–302

Olaizola M, Yamamoto HY (1994) Short-term response of the diadinoxanthin cycle and fluorescence yield to high irradiance in *Chaetoceros muelleri* (Bacillariophyceae). J Phycol 30:606–612

Oldham PB, Zillioux EJ, Warner IM (1985) Spectral "fingerprinting" of phytoplankton populations by two-dimensional fluorescence and Fourier-transform-based pattern recognition. J Plankton Res 43:893–906

Owens T (1986) Light-harvesting function in the diatom *Phaeodactylum tricornutum.* II. Distribution of excitation energy between the photosystems. Plant Physiol 80:739–746

Parésys G, Rigart C, Rousseau B, Wong AWM, Fan F, Barbier J-P, Lavaud J (2005) Quantitative and qualitative evaluation of phytoplankton communities by trichromatic chlorophyll fluorescence excitation with special focus on cyanobacteria. Wat Res 39:911–921

Parkhill JP, Maillet G, Cullen JJ (2001) Fluorescence-based maximal quantum yield for PSII as a diagnostic of nutrient stress. J Phycol 37:517–529

Pope RM, Fry ES (1997) Absorption spectrum (380–700 nm) of pure water. II. Integrating cavity measurements. Appl Opt 36:8710–8723

Poryvkina L, Babichenko S, Kaitala S, Kurosa H, Shalapyonok A (1994) Spectral fluorescent signatures in the characterization of phytoplankton community composition. J Plankton Res 16:1315–1327

Poryvkina L, Babichenko S, Leeben A (2000) Analysis of phytoplankton pigments by excitation spectra of fluorescence. Proceedings of EARSeL-SIG-Workshop LIDAR, Dresden/FRG

Raateoja M, Mitchell BG, Wang H, Olivo E (2009) Effect of water column light gradient on phytoplankton fluorescence transients. Mar Ecol Prog Ser 376:85–101

Ras J, Claustre H, Uitz J (2008) Spatial variability of phytoplankton pigment distributions in the Subtropical South Pacific Ocean: comparison between *in situ* and predicted data. Biogeosciences 5:353–369

Richardson TL, Lawrenz E, Pinckney JL, Guajardo RC, Walker EA, Paerl HW, MacIntyre HL (2010) Spectral fluorometric characterization of phytoplankton community composition using the Algae Online Analyser. Water Research (in press)

Richardson TL, Pinckney JL (2004) Monitoring of the toxic dinoflagellate *Karenia brevis* using gyroxanthin-based detection methods. J Appl Phycol 16:315–328

Roesler CS, Perry MJ (1995) *In situ* phytoplankton absorption, fluorescence emission, and particulate backscattering spectra determined from reflectance. J Geophys Res 100(C7):13279–13294

Ross ON, Moore CM, Suggett DJ, MacIntyre HL, Geider RJ (2008) A model of photosynthesis and photo-protection based on reaction center damage and repair. Limnol Oceanogr 53:1835–1852

Ruban AV, Berera R, Ilioaia C, van Stokkum IHM, Kennis JTM, Pascal AA, van Amerongen H, Robert B, Horton H, van Grondelle R (2007) Identification of a mechanism of photoprotective energy dissipation in higher plants. Nature 450:475–478

Sahay A, Jajoo A, Singh P, Bharti S (2006) Nitrite regulates distribution of excitation energy between the two photosystems by causing state transition. Plant Physiol Biochem 44:7–12

Sakshaug E, Demers S, Yentsch CS (1987) *Thalassiosira oceanica* and *Thalassiosira pseudonana*: two different photoadaptational responses. Mar Ecol Prog Ser 41:275–282

Schimanski J, Beutler M, Moldaenke C, Hansen U-P (2006) A model for correcting the fluorescence signal from a free-falling depth profiler. Water Res 40:1616–1626

Schubert H, Forster RM, Sagert S (1995) *In situ* measurement of state transition in cyanobacterial blooms: kinetics and extent of the state change in relation to underwater light and vertical mixing. Mar Ecol Prog Ser 128:99–108

Sciandra A, Lazzara L, Claustre H, Babin M (2000) Responses of growth rate, pigment composition and optical properties of *Cryptomonas* sp. to light and nitrogen stresses. Mar Ecol Prog Ser 201:107–120

See JH, Richardson TL, Pinckney JL, Shen RJ, Guinasso NL (2005) Combining new technologies for determination of phytoplankton community structure in the northern Gulf of Mexico. J Phycol 41:305–310

Seppälä J, Balode M (1998) The use of spectral fluorescence methods to detect changes in the phytoplankton community. Hydrobiologia 363:207–217

Seppälä J, Olli K (2008) Multivariate analysis of phytoplankton spectral *in vivo* fluorescence: estimation of phytoplankton biomass during a mesocosm study in the Baltic Sea. Mar Ecol Prog Ser 370:69–85

Seppälä J, Ylöstalo P, Kaitala S, Hällfors S, Raateoja M, Maunula P (2007) Ship-of-opportunity based phycocyanin fluorescence monitoring of the filamentous cyanobacteria bloom dynamics in the Baltic Sea. Est Coast Shelf Sci 73:489–500

Serôdio J (2004) Analysis of variable chlorophyll fluorescence in microphytobenthos assemblages: implications of the use of depth-integrated measurements. Mar Ecol Prog Ser 36:137–152

Six C, Thomas JC, Brahamsha B, Lemoine Y, Partensky F (2004) Photophysiology of the marine cyanobacterium *Synechococcus* sp. WH8102, a new model organism. Aquat Microb Ecol 35:17–29

Sosik HM (1988) Analysis of chlorophyll fluorescence in marine phytoplankton: interpretation of flow cytometric signals. Cambridge, MA, Massachussetts Institute of Technology: 88

Sosik HM, Mitchell BG (1991) Absorption, fluorescence, and quantum yield for growth in nitrogen-limited *Dunaliella tertiolecta*. Limnol Oceanogr 36:910–921

Sosik HM, Mitchell BG (1994) Effects of temperature on growth, light absorption, and quantum yield in *Dunaliella tertiolecta* (Chlorophyceae). J Phycol 30:833–840

Spear-Bernstein L, Miller KR (1989) Unique location of the phycobiliprotein light-harvesting pigment in the Cryptophyceae. J Phycol 25:412–419

Staehr PA, Cullen JJ (2003) Detection of *Karenia mikimotoi* by spectral absorption signatures. J Plankton Res 25:1237–1249

Staehr PA, Henriksen P, Markager S (2002) Photoacclimation of four marine phytoplankton species to irradiance and nutrient availability. Mar Ecol Prog Ser 238:47–59

Stolte W, Kraay GW, Noordeloos AAM, Rieman R (2000) Genetic and physiological variation in pigment composition of *Emiliania huxleyi* (Prymnesiophyceae) and the potential use of its pigment ratios as a quantitative physiological marker. J Phycol 36:529–539

Strickland JDH (1968) Continuous measurement of *in vivo* chlorophyll: A precautionary note. Deep Sea Res 15:225–227

Strzepek RF, Harrison PJ (2004) Photosynthetic architecture differs in coastal and oceanic diatoms. Nature 431:689–692

Suggett DJ, MacIntyre HL, Geider RJ (2004) Biophysical and optical determinations of light absorption by photosystem II in phytoplankton. Limnol Oceanogr Methods 2:316–332

Suggett DJ, MacIntyre HL, Kana TM, Geider RJ (2009) Comparing electron transport with gas exchange: parameterising exchange rates between alternative photosynthetic currencies for eukaryotic phytoplankton. Aquat Microb Ecol 56:147–162

Sukenik A, Bennett J, Falkowski PG (1987) Light-saturated photosynthesis – limitation by electron transport or carbon fixation? Biochim Biophys Acta 891:205–215

Sukenik A, Bennett J, Mortain-Bertrand A, Falkowski PG (1990) Adaptation of the photosynthetic apparatus to irradiance in *Dunaliella tertiolecta*. Plant Physiol 92:891–898

Topinka JA, Korjeff Bellows W, Yentsch CS (1990) Characterization of marine macroalgae by fluorescence signatures. Int J Rem Sens 11:2329–2335

Uitz J, HuotY BF, Babin M (2008) Relating phytoplankton photophysiological properties to community structure on large scales. Limnol Oceanogr 53:614–630

van de Hulst HC (1957) Scattering by small particles. Wiley, New York, 470 p

Van Heukelem L, Thomas CS (2001) Computer-assisted high-performance liquid chromatography method development with applications to the isolation and analysis of phytoplankton pigments. J Chromatogr 910:1–49

Verity PG (1981) Effects of temperature, irradiance, and daylength on the marine diatom *Leptocylindrus danicus* Cleve. I. Photosynthesis and cellular composition. J Exp Mar Biol Ecol 55:79–91

Vincent WF (1979) Mechanisms of rapid photosynthetic adaptation in natural phytoplankton communities. I. Redistribution of excitation energy between photosystems I and II. J Phycol 15:429–434

Vincent WF (1980) Mechanisms of rapid photosynthetic adaptation in natural phytoplankton communities. II. Changes in photochemical capacity as measured by DCMU-induced chlorophyll fluorescence. J Phycol 16:568–577

Wright SW, Jeffrey SW, Mantoura RFC, Llewellyn CA, Bjørnland T, Repeta DJ, Welschmeyer NA (1991) Improved HPLC method for the analysis of chlorophylls and carotenoids from marine phytoplankton. Mar Ecol Prog Ser 77:183–196

Yamamoto HY, Bassi R (1996) Carotenoids: localization and function. In: Ort DR, Yocum CF (eds) Oxygenic photosynthesis: the light reactions. Kluwer, The Netherlands, pp 539–563

Yentsch CS, Phinney DA (1985) Spectral fluorescence – an ataxonomic tool for studying the structure of phytoplankton populations. J Plankt Res 7:617–632

Yentsch CS, Yentsch CM (1979) Fluorescence spectral signatures – characterization of phytoplankton populations by the use of excitation and emission-spectra. J Mar Res 37:471–483